Cell

The Permeability of Reconstituted Nuclear Pores Provides Direct Evidence for the Selective Phase Model

Bastian B. Hülsmann,[1] Aksana A. Labokha,[1] and Dirk Görlich[1,*]
[1]Abteilung Zelluläre Logistik, Max-Planck-Institut für biophysikalische Chemie, Am Fassberg 11, D-37077 Göttingen, Germany
*Correspondence: goerlich@mpibpc.mpg.de
http://dx.doi.org/10.1016/j.cell.2012.07.019

SUMMARY

Nuclear pore complexes (NPCs) maintain a permeability barrier between the nucleus and the cytoplasm through FG-repeat-containing nucleoporins (Nups). We previously proposed a "selective phase model" in which the FG repeats interact with one another to form a sieve-like barrier that can be locally disrupted by the binding of nuclear transport receptors (NTRs), but not by inert macromolecules, allowing selective passage of NTRs and associated cargo. Here, we provide direct evidence for this model in a physiological context. By using NPCs reconstituted from *Xenopus laevis* egg extracts, we show that Nup98 is essential for maintaining the permeability barrier. Specifically, the multivalent cohesion between FG repeats is required, including cohesive FG repeats close to the anchorage point to the NPC scaffold. Our data exclude alternative models that are based solely on an interaction between the FG repeats and NTRs and indicate that the barrier is formed by a sieve-like FG hydrogel.

INTRODUCTION

Cell nuclei are enclosed by the nuclear envelope that comprises two concentric membranes and embedded nuclear pores (Watson, 1954). The pores arise from local fusions between inner and outer nuclear membranes (reviewed in Hetzer and Wente, 2009). They connect the nuclear interior with the cytoplasm and are integrated into giant protein structures of 8-fold rotational symmetry called nuclear pore complexes (NPCs).

NPCs pose efficient barriers for inert objects $\geq$5 nm in diameter (Mohr et al., 2009). They suppress an intermixing of nuclear and cytoplasmic contents, which in turn is a requirement for the ordered course of eukaryotic gene expression. Shuttling nuclear transport receptors (NTRs), however, can cross the barrier in a highly facilitated manner (reviewed in Görlich and Kutay, 1999). NTRs bind cargo molecules and supply nuclei with proteins and the cytoplasm with nuclear products like ribosomes. The facilitated mode of NPC passage reaches a capacity of up to 1,000 translocation events per NPC per second (Ribbeck and Görlich, 2001) and accommodates objects of up to nearly 40 nm in diameter (Panté and Kann, 2002; Lowe et al., 2010). NTRs can utilize an energy input, e.g., from the RanGTPase system to accumulate substrates against steep concentration gradients (Görlich et al., 2003). In addition, directional transport requires an intact NPC barrier that retains the transported molecules inside the destination compartment.

NPCs are built from ~30 different nucleoporins (Nups) that can be classified into structural Nups and phenylalanine-glycine repeat-containing Nups (FG Nups). The structural Nups form the NPC scaffold and provide binding sites for the FG Nups (reviewed in Brohawn et al., 2009). FG domains (Hurt, 1988) are essential for viability and are critical for the barrier (Strawn et al., 2004; Frey and Görlich, 2007; Patel et al., 2007). They represent nonglobular protein structures (Denning et al., 2003), typically comprising hundreds of residues and containing up to 50 FG, FxFG, or GLFG motifs (here collectively called FG motifs).

FG motifs bind NTRs during facilitated translocation (Iovine et al., 1995; Radu et al., 1995; Rexach and Blobel, 1995; Bayliss et al., 1999; Isgro and Schulten, 2005). It is, however, not trivial to explain how such interactions render NPCs 100- to >1,000-fold more permeable for NTR•cargo complexes than for inert objects of similar size. In fact, a mere binding of NTRs to FG motifs should cause retention of NTR•cargo complexes and thus delay their passage through the central NPC channel. More importantly, such a simple arrangement cannot explain why molecules that are not bound to an NTR are blocked from NPC passage.

To resolve this "nuclear transport paradox," we previously proposed the "selective phase model" (Ribbeck and Görlich, 2001; see Figure 1). It assumes that the barrier-forming FG domains comprise many cohesive units, which bind each other and thereby mediate multivalent interactions within but also between individual FG domains. Such interactions would result in a sieve-like FG hydrogel (the selective phase) that allows passage of small molecules but suppresses fluxes of larger ones. NTRs overcome this size limit by binding to FG motifs and consequently disengaging FG meshes in their immediate vicinity (Ribbeck and Görlich, 2001; Kustanovich and Rabin, 2004). This way, NTRs can partition into the FG hydrogel and eventually exit the barrier on the *trans* side.

The selective phase model is supported by several observations. First, yeast NPCs contain numerous cohesive FG domains

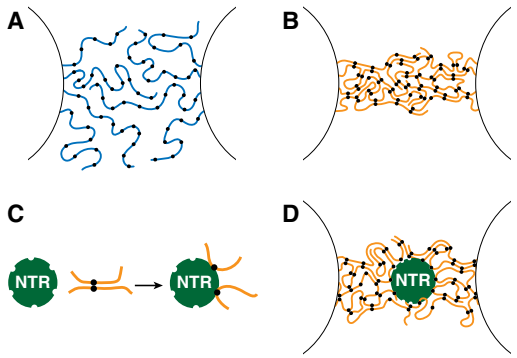

Figure 1. Scenarios for Noncohesive and Cohesive FG Domains

(A) Scenario in which the NPC channel contains only FG domains that do not interact with each other. "●" denotes FG motifs, i.e., binding sites for NTRs. According to the virtual gate model, such noncohesive FG brushes repel inert material.

(B) Scenario in which highly cohesive FG domains interact multivalently with each other to form a sieve-like hydrogel, the proposed selective phase. The mesh size would set an upper size limit for unhindered NPC passage of inert material.

(C) According to the selective phase model, NTRs not only bind FG motifs but also disengage repeat-repeat interactions. This transiently opens meshes in the immediate vicinity of NTRs.

(D) Passage of an NTR through an FG hydrogel.

(Frey and Görlich, 2007, 2009; Patel et al., 2007). Second, sufficiently concentrated solutions of cohesive FG domains spontaneously form FG hydrogels (Frey et al., 2006; Frey and Görlich, 2009; Milles and Lemke, 2011). Third, cargo•NTR complexes migrate into such hydrogels up to 20,000-fold faster than the respective cargoes alone (Frey and Görlich, 2007, 2009). Fourth, the intragel diffusion rate of a typical importin-β•cargo complex predicts a similar NPC passage time (~10 ms) as was observed for traversing authentic NPCs (Yang et al., 2004; Kubitscheck et al., 2005; Frey and Görlich, 2007).

Nevertheless, it is still unclear whether FG domains behave at the nanoscopic scale of an NPC the same way as in macroscopic hydrogels and whether the function of authentic NPCs indeed relies on inter-FG cohesion and, hence, on hydrogel formation. A number of alternative models have been suggested. The "reduction of dimensionality model" (Peters, 2005), for example, assumes that the central NPC channel is narrow enough to effectively suppress three-dimensional random walks of inert material through the pore, whereas NTRs (with bound cargo) are postulated to reach the other channel side faster by sliding two-dimensionally along an FG-covered channel surface. The "virtual gate model" (Rout et al., 2003) also does not rely on inter-FG cohesion. Instead, it assumes that the brush-like behavior of (otherwise noninteracting) FG domains is sufficient to repel inert material from the central channel and that NTRs overcome this repulsion by binding to FG motifs. The "reversible collapse model" (Lim et al., 2007) is identical to the virtual gate model up to the point that FG brushes repel inert material, but it further assumes that FG domains contract upon NTR binding and thereby move cargo complexes across the barrier.

The field of nuclear transport is currently discussing which of the models describes the fundamental principles of the NPC barrier correctly. There is, however, general agreement that only tests in the context of real NPCs can provide a valid decision (Weis, 2007; Terry and Wente, 2009; Wälde and Kehlenbach, 2010; Tu and Musser, 2011). Fortunately, the various models differ clearly in their predictions as to how changes in the properties of FG domains would impact NPC selectivity. The selective phase, virtual gate, and reversible collapse models predict a barrier collapse when FG domains are removed, whereas the reduction of dimensionality model predicts little effect on passive NPC passage. The selective phase model predicts an NPC barrier failure when cohesive FG repeats are replaced by noncohesive ones, whereas all the other mentioned models predict no impact.

We have now developed a system, based on engineered NPCs, that allows testing such predictions. We found that the passive diffusion barrier of vertebrate NPCs depends crucially on the FG nucleoporin Nup98 and, in particular, on its FG domain. We further observed that the isolated Nup98 FG domain is highly cohesive and forms FG hydrogels of exquisite NPC-like selectivity. Nonselectively permeable NPCs were evident when the Nup98 FG domain had been exchanged for any noncohesive FG domain. This also applied to noncohesive domains that were fully proficient in NTR binding. In contrast, heterologous highly cohesive FG domains allowed NPCs to exclude large inert molecules and to mediate efficient active transport. Our findings suggest that inter-FG cohesion is fundamental for NPC function and lend strong support to the selective phase model.

RESULTS

The central predictions of the selective phase model are that the NPC-barrier-forming FG domains are cohesive and that replacing these cohesive FG domains by noncohesive ones leads to a barrier failure. We wanted to test these predictions in authentic NPCs. This required us to identify the barrier-relevant FG domain(s) and to establish a system that allows exchanging FG domains and subsequently monitoring of the permeability properties of the resulting NPCs. *Xenopus laevis* egg extracts appeared to be an ideal starting point. They are a rich source for nuclear membrane precursors and soluble Nups, allowing de novo assembly of nuclei around templates of demembranated sperm chromatin (Forbes et al., 1983; Lohka and Masui, 1983; Blow and Laskey, 1986). Importantly, individual Nups can be removed before assembly and replaced by engineered versions. The critical advantage of this system over genetic approaches is that it allows analysis of the full spectrum of NPC permeability phenotypes, i.e., even of those that would be lethal in a cellular context. Nuclei assembled from nondepleted extract behaved as expected. They excluded a variety of inert macromolecules and showed active import of IBB-MBP, which represents a fusion between a strong importin-β-dependent import signal (the IBB domain; Görlich et al., 1996) with the maltose-binding protein from *Escherichia coli* (MBP). Likewise, they showed CRM1-mediated export of a nuclear export signal (NES) fused to GFP. This together indicated that the newly assembled NPCs had gained both an intact passive permeability barrier and the competence for facilitated translocation (Figures 2D and S2 available online).

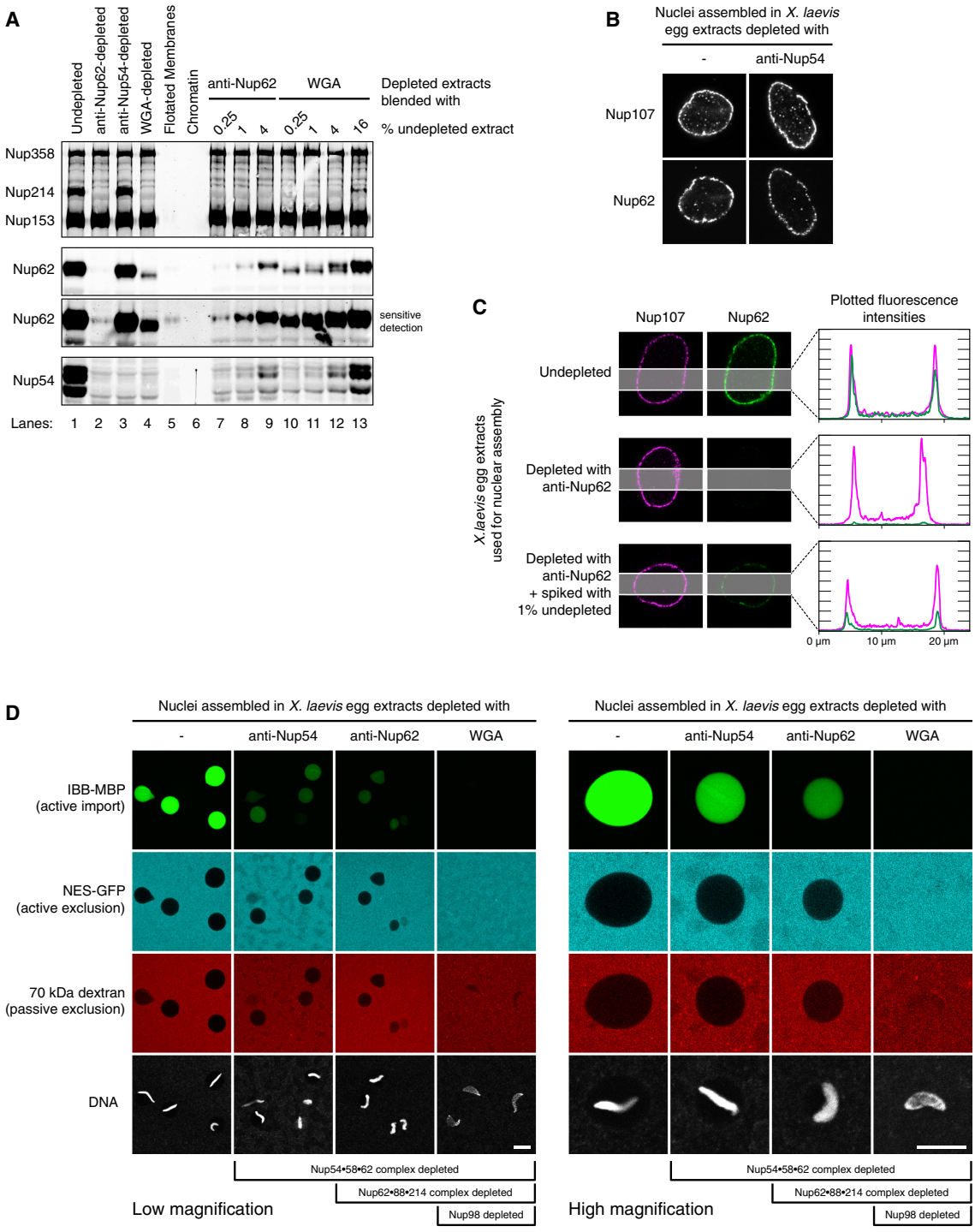

Figure 2. Depletion of Nup62 Complexes Leaves the NPC Barrier Largely Intact

X. laevis egg extracts were depleted by using anti-Nup54 to remove the Nup54•58•62 complex, anti-Nup62 to remove the Nup54•58•62 and Nup62•88•214 complexes, or WGA to deplete all O-GlcNAc-modified nucleoporins. The specificity of antibodies is also shown in Figure S1.

(A) Immunoblot analysis of the components used for nuclear assembly. The endogenous FG nucleoporins Nup358, Nup214, Nup153, and Nup62 were detected by mAB414. The various isoforms of Nup54 were detected by rabbit anti-Nup54. For quantification, depleted cytosols were blended with increasing amounts of undepleted cytosol. A Nup62 signal became detectable upon readdition of as little as 0.25% undepleted extract to a Nup62-depleted extract (compare lanes 2 and 7). This matches the quantification by integrating fluorescent signals (not shown). Thus, anti-Nup62 depleted the two Nup62 complexes to residual levels of no more than 0.25%. Those complexes were also depleted with WGA (lane 4). Membranes prepared by conventional methods contained soluble nucleoporins unless they were further purified by flotation (see Figure S1D).

The Nup62 Complexes Appear Dispensable for Basic NPC Function

We first tested the contribution of Nup62 (Finlay et al., 1991) to the NPC barrier because it is well conserved and localized to the center of the central NPC channel (Grote et al., 1995), where a selectivity filter would be most effective. Also, it probably represents the FG Nup with the highest copy number (Cronshaw et al., 2002). It occurs in two complexes. The Nup54•58•62 complex (Finlay et al., 1991; Hu et al., 1996) contributes four FG domains with a combined length of 836 residues, whereas the Nup62•88•214 complex (Macaulay et al., 1995; Fornerod et al., 1997) provides two FG domains with a combined length of 1,165 residues. Surprisingly, depletion of the Nup54•58•62 complex or the simultaneous depletion of the Nup54•58•62 and Nup62•88•214 complexes did not eliminate the NPC barrier. The nuclei appeared smaller, displayed a still respectable, albeit clearly reduced, facilitated import activity, and showed passive as well as active CRM1-mediated exclusion (Figures 2D and S2). These nuclei even replicated their DNA (Figure S2C).

It is possible that an insufficient degree of depletion accounts for a lack of more severe defects, in particular, as the source extract contains more Nup62 than needed to saturate its NPC binding sites. We regard this, however, as unlikely. Compared to their original concentration, the Nup62 complexes were depleted to very low levels, namely to $\leq$0.2% in the extract (Figure 2A) and to ~1% in assembled NPCs (Figure 2C; data not shown). This indeed rules out that the basic functions of the NPC barrier have a stoichiometric requirement for the Nup62 complexes.

These results are in contrast to the so-far prevailing view that Nup62 complexes are essential for NPC function (Finlay et al., 1991). They are, however, in line with the observation that deleting the NPC binding site for Nsp1p (the yeast ortholog to Nup62) on Nic96p causes a growth defect, but not lethality (Schrader et al., 2008).

Nup98 Is Essential for Active Transport and the Passive Barrier

A drastic phenotype, however, became evident when all O-GlcNAc-modified FG Nups (Nups 54, 58, 62, 98, and 214) were depleted with the immobilized lectin wheat germ agglutinin (WGA; Finlay and Forbes, 1990). The resulting nuclei displayed a closed nuclear envelope (data not shown) and contained NPCs that stained positively for nondepleted Nups (Figures 4C, 7A, S2C, and S4; data not shown) but failed in active nuclear import and export (see e.g., Figures 2D, 4A, and 7A–7C) as well as in DNA replication (Figure S2C). This is in full agreement with previous reports (Finlay and Forbes, 1990). Importantly, these WGA-depleted NPCs also failed to exclude fluorescently labeled large inert molecules, such as a 70 kDa dextran or IgGs (Figures 2D and S2B), indicating that they did not maintain a permeability barrier.

The WGA depletion phenotype was previously attributed to the loss of Nup62 complexes (Finlay et al., 1991). Our observation that depletion with anti-Nup62 resulted in lower residual Nup62 levels than the WGA depletion and yet produced milder defects, however, argues against this conclusion. Instead, it appears that the depletion of an additional component by WGA is responsible for the drastic phenotype. One candidate is Nup98 (Powers et al., 1995; Radu et al., 1995), previously also called p97. This would be consistent with the recent suggestion that phosphorylation of Nup98 is crucial for mitotic disassembly of the NPC barrier (Laurell et al., 2011). As expected for a critical barrier constituent, Nup98 shows a very central localization within the NPC channel (Krull et al., 2004). Furthermore, it is heavily O-GlcNAc modified and is removed upon WGA depletion (Powers et al., 1995; Figures 3A and 3D). To test whether Nup98 is indeed this critical component, we asked whether the barrier defects are revertible by readdition of Nup98.

To this end, we recombinantly expressed Nup98 in *E. coli*—a host lacking nuclei and thus any Nups that could possibly contaminate the preparation. Previous expression attempts were hampered by the fact that Nup98 is very insoluble when expressed in bacteria (Hodel et al., 2002), probably because its cohesive FG domain (see below) engages in interchain contacts and thus causes poor water solubility. We solved this problem by fusing in front of Nup98 a very large and water-soluble (His_{14}-MBP-SUMO) tag that apparently provides sufficient shielding to prevent the formation of large aggregates (Figure 3C). We left the tag on the protein during the complete purification procedure. The tag, however, was cleaved upon addition to the egg extract, which contains not only the cleaving SUMO protease (Li and Hochstrasser, 1999) but also chaperones that keep mature Nup98 soluble. Figure 3D documents this processing as well as the faithful O-GlcNAc modification of recombinant Nup98 by activities present in the egg extract. Importantly, readdition of Nup98 restored not only active nuclear transport into WGA-depleted nuclei but also the passive permeability barrier (Figures 4A and S3A), proving Nup98 as a critical barrier component. The level of activity was comparable to that of nuclei lacking the Nup62 complexes (Figure 2D).

(B–D) Nuclei were assembled from *Xenopus* sperm chromatin, membranes, and interphase egg extracts that had been depleted as indicated. (B and C) Nuclei were fixed and analyzed by immunofluorescence (IF) with indicated NPC markers. The Nup62 signal remaining after anti-Nup54 depletion can be assigned to the nondepleted Nup62•88•214 complex. The Nup107 signal indicates that depletions of Nup62-containing complexes did not interfere with assembly of the NPC scaffold. Nup62 depletions were further analyzed by line profiles. Note that addition of as little as 1% undepleted extract lead to reappearance of a nuclear rim signal. (D) Test of NPC barrier function in assembled nuclei. Nucleocytoplasmic distributions of fluorescent permeation probes were recorded by confocal scans through unfixed transport reactions. Left and right panels derive from an identical experiment but were imaged at different magnifications. WGA-depleted nuclei failed in active import and export as well as in dextran exclusion. Scale bars, 25 μm. Further data on depletion phenotypes are provided in Figure S2.
In transport-competent nuclei, the DAPI-stained chromatin did not necessarily fill the complete nuclear interior. This represents a well-documented peculiarity of the amphibian nuclear assembly system that becomes most obvious after longer incubation times (see e.g., Figure 7A in Lu et al., 1997). It probably relates to the facts that in-vitro-assembled nuclei are an early embryonic type whose nuclear organization is optimized for extremely rapid cell cycles and that early embryonic chromatin is transcriptionally inactive and might therefore relapse to a more condensed state once replication is completed.

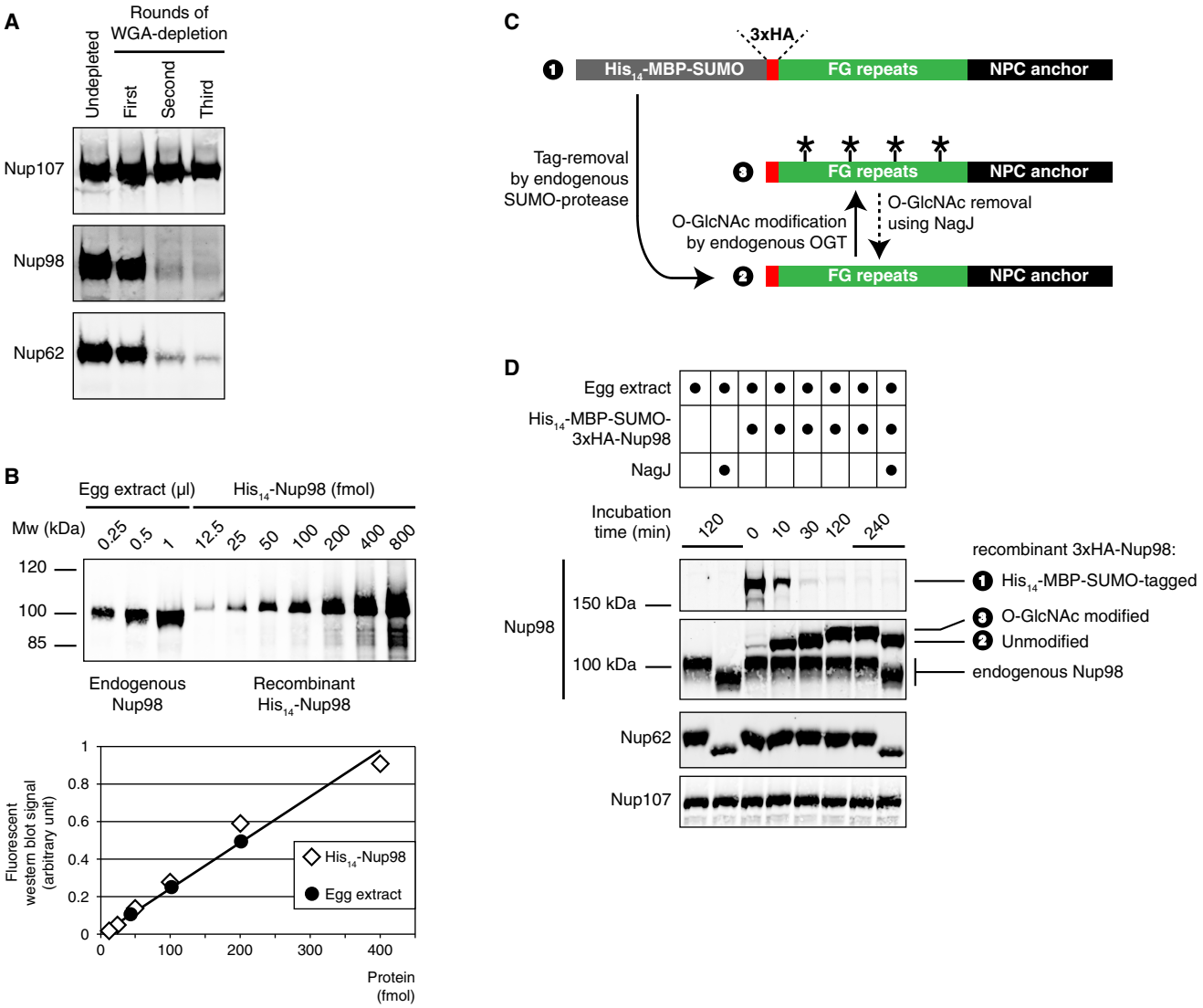

Figure 3. Recombinant Production and Enzymatic Modification of Nup98

(A) Immunoblot analysis of WGA-depleted extracts that provide an assay for Nup98 function. Samples were taken after each round of WGA depletion and analyzed by immunoblotting. The final extract was used for functional assays.

(B) Quantification of endogenous Nup98. Anti-Nup98 was used to detect the endogenous protein as well as the recombinant standard. The concentration of endogenous Nup98 in nondepleted extract was determined by comparative immunoblotting to be 200 nM.

(C) Scheme of posttranslational processing of recombinant Nup98 during incubation with egg extract. SUMO protease from the extract cleaves off the His_{14}-MBP-SUMO module, generating a 3xHA-Nup98 fusion (2) that is subsequently modified by O-GlcNAc-transferase (OGT) to yield an O-GlcNAc-modified form of 3xHA-Nup98 (3). NagJ is a bacterial glycosidase (Rao et al., 2006) that can remove the O-GlcNAc modifications from Nup98.

(D) 200 nM His_{14}-MPB-SUMO-3xHA-Nup98 were incubated in egg extract, and aliquots were analyzed by immunoblotting. Anti-Nup98 recognizes both the endogenous and all types of the added recombinant Nup98. 3xHA-tagged Nup98 is 3.5 kDa larger than endogenous Nup98. Anti-Nup62 and anti-Nup107 served as additional controls.

As a next step, we asked whether Nup98 is also required when NPCs retain wild-type levels of all the other FG Nups, including Nup62. To this end, we used antibodies against Nup98 for depletion. Nup98-depleted nuclei were indeed incapable of actively accumulating an IBB-MBP fusion protein (Figures 4B and S3A), as expected for NPCs that cannot suppress the backflow of previously imported molecules. Again, these defects were reverted by readdition of recombinant Nup98 (Figures 4B and S3A). The level of restoration matched the activity of nondepleted nuclei.

The FG Domain of Nup98 Forms a Highly Selective Barrier In Vitro

Considering the crucial contribution of Nup98 to the vertebrate NPC barrier, we next wanted to know whether the Nup98 FG domain would form a hydrogel and, if so, which barrier properties

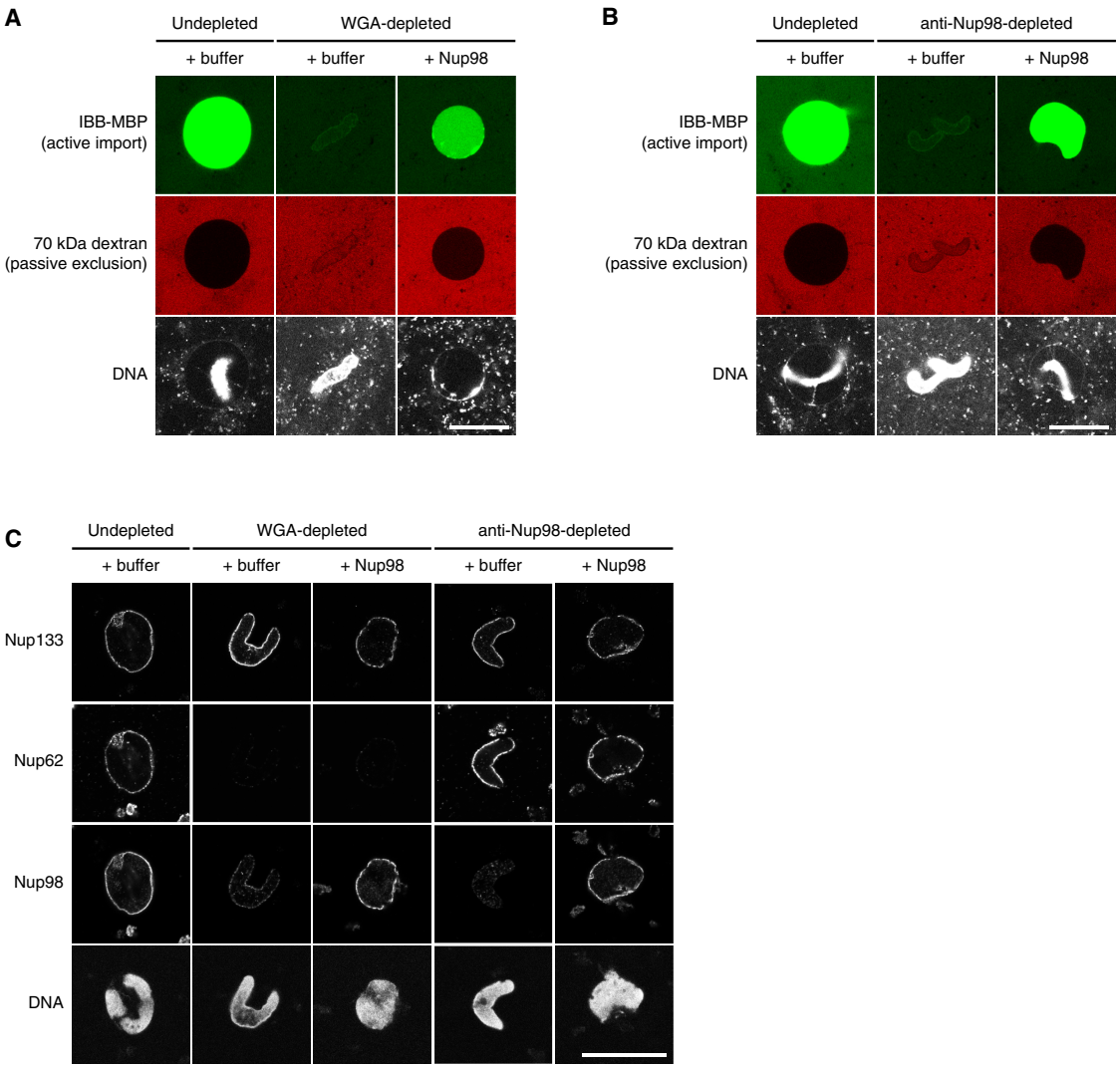

Figure 4. Nup98 Dominates the Permeability Barrier of *Xenopus* NPCs

Nuclei were assembled as in Figure 2 using depleted or nondepleted egg extracts. Recombinant *Xenopus* Nup98 was added to its original endogenous concentration of 200 nM (Figure 3B).

(A and B) Nup98 restores passive nuclear exclusion and active import in WGA- and Nup98-depleted nuclei. See also Figure S3A.

(C) Composition of depleted and restored NPCs. Nuclei characterized in (A) and (B) were fixed and analyzed by IF with indicated NPC markers. Note that the low level of residual Nup98 in WGA-depleted NPCs was insufficient for an operational permeability barrier.

Scale bars, 25 μm.

such gel displays. To this end, the 485-residue-long *Xenopus* FG domain ($Nup98^{1–485}$) was bacterially expressed, purified, and incubated with UDP-GlcNAc and O-GlcNAc transferase to introduce the typical O-GlcNAc modifications. When dissolved at 200 mg/ml in physiological buffer, it formed a transparent FG hydrogel of very high, NPC-like selectivity (Figures 5A and 5C–5E). The gel fully excluded the 80 kDa passive permeation marker MBP-mCherry but at the same time allowed at least 5,000 times faster influx of a 185 kDa importin-β•IBB-MBP-GFP complex. Considering that NTR influx is limited by diffusion from the buffer to the gel surface (data not shown, but see Figure 2 in Frey and Görlich [2007]), the NTR•cargo complex actually entered the gel about 20,000 times faster than the passive diffusion marker. It is thus plausible to assume that a layer of such a gel inside the central NPC channel accounts for the observed physiological transport selectivity of NPCs.

Restoring a Functional Barrier in WGA-Depleted NPCs Requires the Nup98 FG Domain

We next wanted to know whether the gel-forming FG domain is required for Nup98 function. For that, we produced a ΔFG Nup98 variant ($Nup98^{486–866}$). Importantly, ΔFG Nup98 failed to restore the permeability barrier of WGA-depleted NPCs at any concentration, i.e., even when its binding sites at NPCs had been saturated (Figures 6A and S4; data not shown). Thus, introducing a functional barrier in WGA-depleted NPCs required

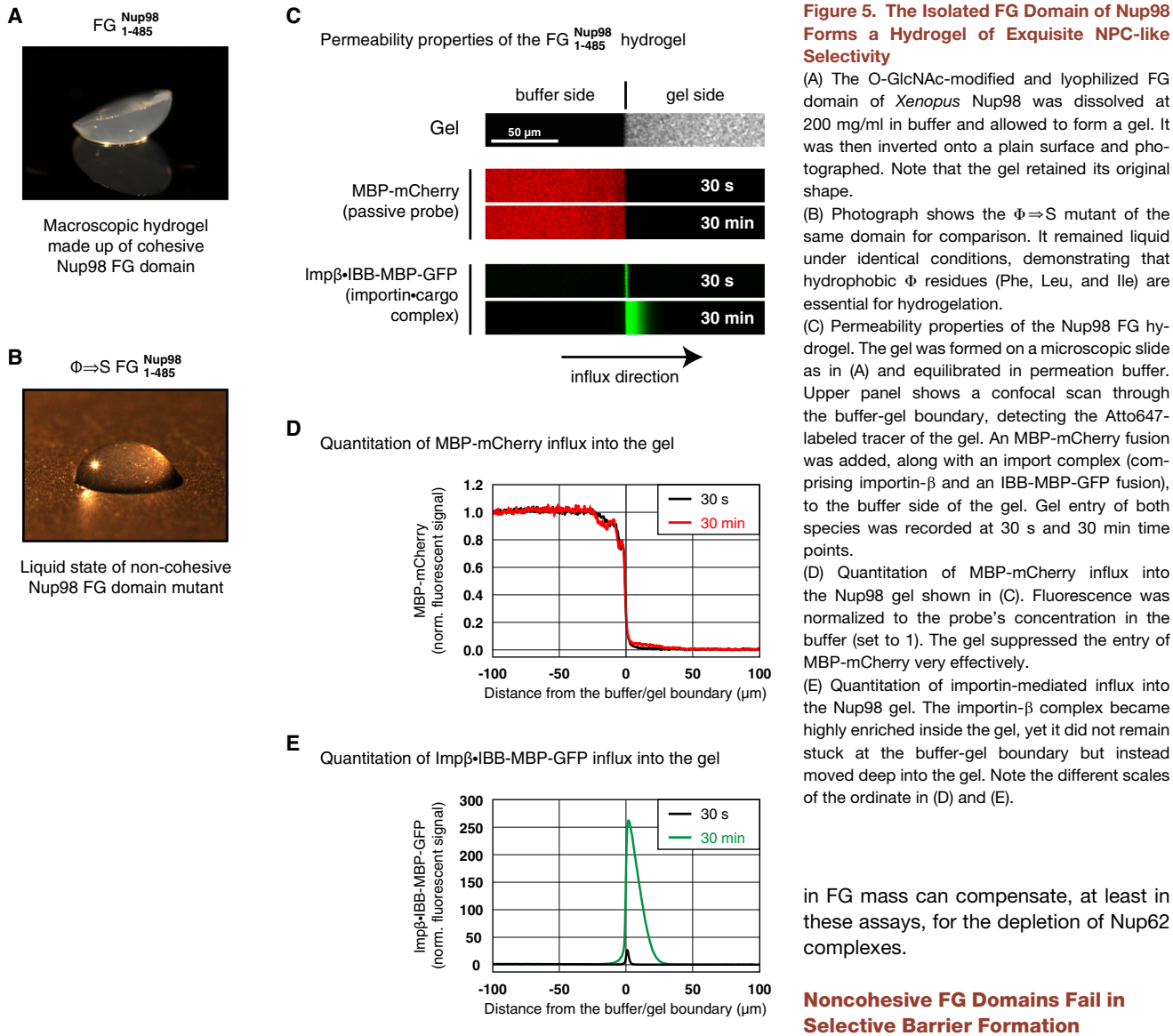

Figure 5. The Isolated FG Domain of Nup98 Forms a Hydrogel of Exquisite NPC-like Selectivity

(A) The O-GlcNAc-modified and lyophilized FG domain of *Xenopus* Nup98 was dissolved at 200 mg/ml in buffer and allowed to form a gel. It was then inverted onto a plain surface and photographed. Note that the gel retained its original shape.

(B) Photograph shows the Φ⇒S mutant of the same domain for comparison. It remained liquid under identical conditions, demonstrating that hydrophobic Φ residues (Phe, Leu, and Ile) are essential for hydrogelation.

(C) Permeability properties of the Nup98 FG hydrogel. The gel was formed on a microscopic slide as in (A) and equilibrated in permeation buffer. Upper panel shows a confocal scan through the buffer-gel boundary, detecting the Atto647-labeled tracer of the gel. An MBP-mCherry fusion was added, along with an import complex (comprising importin-β and an IBB-MBP-GFP fusion), to the buffer side of the gel. Gel entry of both species was recorded at 30 s and 30 min time points.

(D) Quantitation of MBP-mCherry influx into the Nup98 gel shown in (C). Fluorescence was normalized to the probe's concentration in the buffer (set to 1). The gel suppressed the entry of MBP-mCherry very effectively.

(E) Quantitation of importin-mediated influx into the Nup98 gel. The importin-β complex became highly enriched inside the gel, yet it did not remain stuck at the buffer-gel boundary but instead moved deep into the gel. Note the different scales of the ordinate in (D) and (E).

the FG domain of Nup98. This might be surprising, as multiple FG domains must be deleted to impair NPC function in *S. cerevisiae* (Strawn et al., 2004). However, this yeast contains three Nup98-like molecules, namely Nup100, Nup116, and Nup145N, which explains the observed redundancy.

The Highly Cohesive FG Domains of Yeast Nup100 and Nup116 Also Form a Functional NPC Barrier

We next asked whether any heterologous FG domain can restore the barrier function when fused to ΔFG Nup98. Indeed, chimeras containing the highly cohesive FG repeats of either *S. cerevisiae* scNup100p or scNup116p (Wente et al., 1992; Patel et al., 2007) rescued passive exclusion and active import in WGA-depleted nuclei even more efficiently than authentic Nup98 (Figures 6A and S4). These heterologous FG domains are longer than the original Nup98 FG domain, and it thus appears that an increase in FG mass can compensate, at least in these assays, for the depletion of Nup62 complexes.

Noncohesive FG Domains Fail in Selective Barrier Formation

Having a functional assay for barrier-forming FG domains at hand, we could now test whether inter-FG cohesion is essential for NPC function. Hydrophobic interactions are crucial for inter-FG cohesion (Frey et al., 2006; Patel et al., 2007; Ader et al., 2010). We therefore mutated all hydrophobic Φ residues (Phe, Leu, and Ile) of the Nup98 FG domain to serines and obtained a Φ⇒S mutant that is fully negative in FG hydrogel formation (Figure 5B). Strikingly, the Nup98 Φ⇒S FG domain mutant also failed to restore the passive permeability barrier of WGA-depleted NPCs (Figures 6C and S7).

The incorporation of Nup98 into NPCs is favored by avidity effects (see below and Griffis et al., 2003). These probably arise because NPCs incorporate many copies of Nup98 simultaneously and because FG-repeat-mediated cohesion between individual Nup98 molecules renders them into multivalent NPC ligands. The noncohesive Φ⇒S mutant not only lacks such avidity contribution, but its NPC binding might be further

disfavored by the entropic volume exclusion effects expected for such an extended hydrophilic sequence. The latter effect would explain why the Φ⇒S Nup98 mutant binds NPCs weaker than the ΔFG variant (Figure S6). Adding a higher concentration of the mutant nevertheless allowed saturation of its binding sites. Alternatively, we mimicked the avidity contribution by fusing a tetramerizing leucine zipper (Harbury et al., 1993) in front of the mutated FG domain. With that, we observed wild-type occupancy of the Φ⇒S Nup98 mutant even at nanomolar concentrations (Figures 6C and S6). Strikingly, however, the passive permeability barrier was not restored (Figures 6C and S7), supporting the assumption that the barrier normally relies on interrepeat cohesion.

Because the noncohesive Φ⇒S mutant lacks FG motifs, it appeared, however, also possible that a lack of NTR binding (Figure 6B) caused the barrier defect. If this were true, then we should see complementation with noncohesive repeats that are proficient in NTR binding. Residues 274–601 of the yeast nucleoporin scNsp1p (Hurt, 1988) exemplify an FG domain with such properties. Its FG motifs bind NTRs very efficiently (see e.g., Clarkson et al., 1996; Bayliss et al., 2000; Figure 6B), but their highly charged inter-FG spacers render the scNsp1$^{274–601}$ FG domain noncohesive (Ader et al., 2010; Yamada et al., 2010). We fused this domain singly or as a tandem dimer, with or without the leucine zipper, to the ΔFG Nup98 module, yielding scNsp1$^{274–601}$ Nup98 chimeras. Strikingly, none of these noncohesive chimeras restored the permeability barrier of WGA-depleted NPCs (Figures 6C and S7; data not shown), even under conditions that led to their efficient incorporation into NPCs (Figures 6C and S6).

The Only Partially Cohesive FG Domain from Nsp1p Also Fails to Provide a Barrier in NPCs

The complete FG domain of scNsp1p (scNsp1p$^{1–601}$) contains not only noncohesive repeats (scNsp1p$^{274–601}$) but also a shorter, highly cohesive part (scNsp1p$^{1–175}$; Ader et al., 2010). The natural combination of the two segments (ScNsp1p$^{1–601}$) forms highly selective FG hydrogels in vitro (Frey and Görlich, 2007). As a fusion to the Nup98 anchor, however, it failed to create a functional permeability barrier when added to WGA-depleted NPCs (Figures 7A, 7C, and S3B). One explanation for this difference is that the FG domain can adopt all orientations in the macroscopic gel, but when anchored to the NPC wall, the long noncohesive region might create a thick layer of high permeability around the NPC anchor points, which then renders the entire NPC leaky (illustrated in Figure 7D; see Discussion).

If this were true, then a replacement of the noncohesive part with cohesive FG repeats should amend the problem. Indeed, a Nup98 chimera containing four copies of the highly cohesive scNsp1p N terminus (scNsp1p$^{2–175}$) yielded functional NPCs (Figures 7A and S3B). This is remarkable because the Nsp1p$^{2–175}$ domain shows only little similarity to the original Nup98 FG sequence. Nup98 is a GLFG nucleoporin, whereas Nsp1p$^{2–175}$ lacks GLFG motifs and instead relies on deviating FG patterns. Also, Nsp1p$^{2–175}$ has extremely N/Q-rich inter-FG spacers, whereas the Nup98 FG domain has an N/Q content close to average proteins and thus achieves high cohesiveness apparently by a greater contribution from hydrophobic residues. This suggests that the specific primary sequence of FG repeat units may not be important. Rather, collective properties might be critical, such as a high propensity to form a narrow-meshed FG hydrogel and the presence of motifs that allow NTRs to transiently disengage inter-FG contacts.

Cohesiveness of FG Domains Is Required, Even in NPCs with an Increased Number of Anchor Points

WGA-depleted NPCs, complemented with Nup98 chimera, lack Nup62 complexes and thus contain fewer FG anchor points than usual. Moreover, the depletion of the Nup62•88•214 complex probably also removed one Nup98 anchor point (Griffis et al., 2003). This would leave perhaps no more than two Nup98 binding sites per NPC asymmetric unit (one for each copy of the Nup107–160 complex; see Belgareh et al., 2001 and Vasu et al., 2001). At this point, it could not be excluded that noncohesive repeats would become functional if only they had more anchor points at NPCs. To explore this possibility, we tested several FG domains at a higher copy number. For that, we chose a modified Nup54•58•62 complex as a second anchor point. We deleted its FG domains and prepared a recombinant ΔFG Nup54•58•62 complex. This complex assembled very efficiently into WGA-depleted NPCs; however, we could not detect effects on Nup98-supplemented WGA-depleted NPCs (data not shown).

In a second step, we converted the ΔFG Nup62 complex into a docking site for Nup98 chimeras. For that, we fused the Nup98 binding site of the Nup107–160 complex (residues 1–19 of Nup96; "96N"; Hodel et al., 2002) to the N terminus of ΔFG Nup62. The resulting 96N-ΔFG Nup62 complex now acted in a highly synergistic manner with added Nup98. WGA-depleted nuclei complemented with Nup98 in the presence of the 96N-ΔFG Nup62 complex showed a much higher level of IBB-MBP accumulation than those complemented by Nup98 alone (Figure 7B). Importantly, however, additional anchor points provided by 96N-ΔFG Nup62 complexes did not render functional those Nup98 chimeras that contained the noncohesive 2xNsp1p$^{274–601}$ or the partially cohesive Nsp1p$^{1–601}$ domains. These reconstituted nuclei still failed in active import and passive exclusion (Figure 7C). NPCs harboring the 96N-Nup62 anchor and the Nup98 chimera containing the all-cohesive 4xNsp1p$^{2–175}$ module, however, showed efficient passive exclusion and robust active import (Figure 7C).

DISCUSSION

NPCs are the central players in a sophisticated barrier system that controls the distribution of macromolecules between the nucleus and the cytoplasm. They keep a barrier against passive diffusion and at the same time conduct facilitated transport. Both functions are, however, intimately linked (1) because the barrier prevents an uncontrolled dissipation of the nucleocytoplasmic RanGTP gradient (that drives all importin- and exportin-mediated transport cycles); (2) because the barrier prevents a backflow of actively transported cargoes from the destination compartment; and (3) because it is the passive barrier that needs

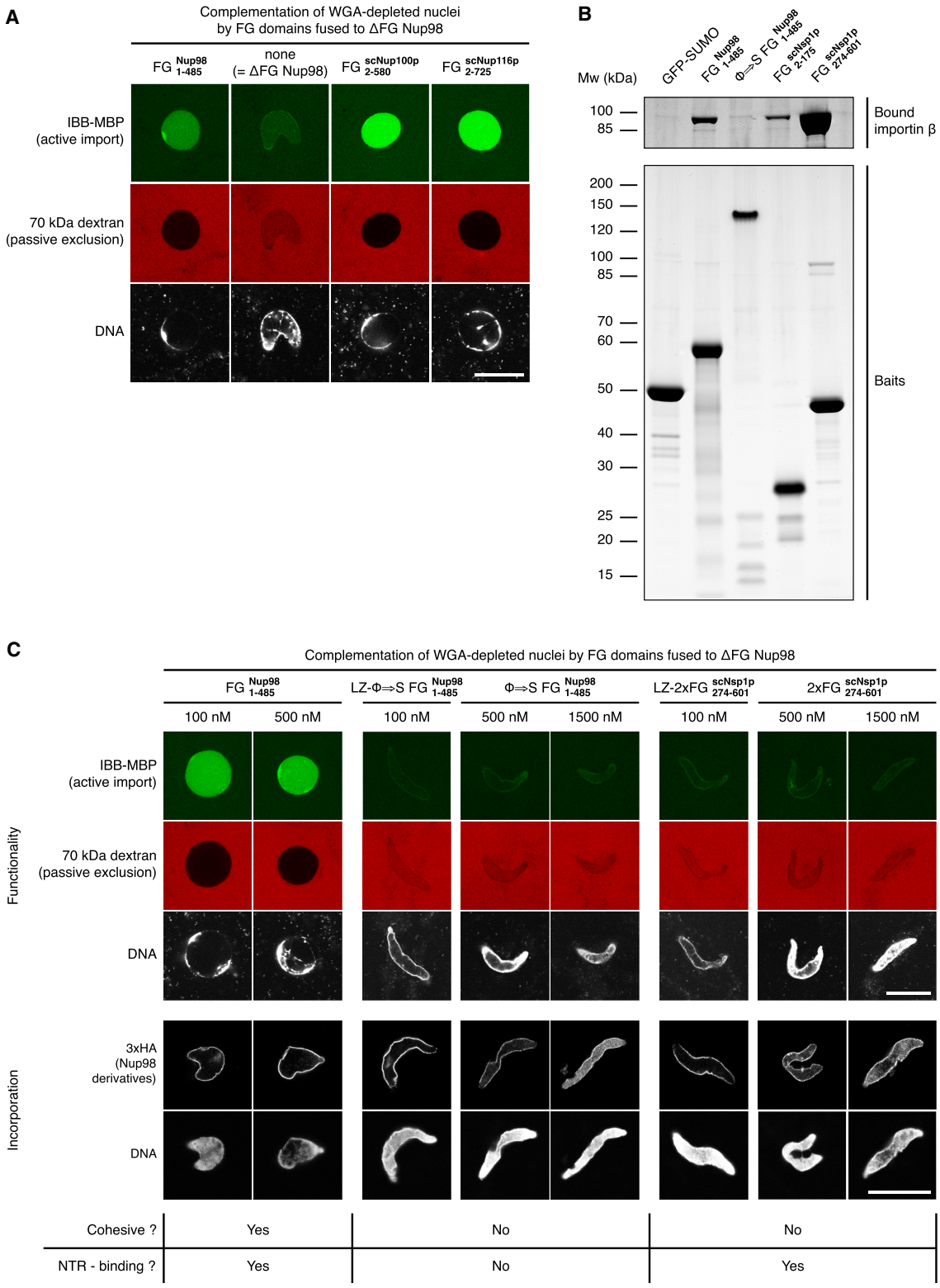

Figure 6. Only Cohesive FG Domains Create a Functional NPC Barrier

(A) WGA-depleted egg extracts were complemented with indicated Nup98 derivatives and were used for nuclear assembly. Passive dextran exclusion and active nuclear import were evident when ΔFG Nup98 had been fused to highly cohesive repeats of either *Xenopus* Nup98 or *S. cerevisiae* Nup100 or Nup116. See Figure S4 for additional data.

to be traversed during facilitated transport. There is general agreement that FG domains bind NTRs during facilitated NPC passage and that this interaction is absolutely critical for this process. We now demonstrate that inter-FG repeat cohesion is equally important, providing compelling evidence for the selective phase model.

The model assumes that the barrier-forming FG domains assemble into a sieve-like meshwork that excludes inert molecules $\geq$5 nm in diameter but allows NTR•cargo complexes to pass. NTRs possess multiple FG binding sites. They use them to rapidly dissolve adjacent inter-FG repeat contacts and consequently to "melt" through the gel. While this happens, the gel seals tightly around the translocating species, which ensures that the barrier keeps excluding irrelevant macromolecules, even when NPCs conduct a heavy load of facilitated translocation.

Our previous and current experiments with purified proteins demonstrated that cohesive FG repeats can form hydrogels that display all the barrier properties expected for authentic NPCs; the gels allow NTR•cargo complexes to move through but constitute an effective barrier toward inert molecules (Frey and Görlich, 2007, 2009). We now also show that these conclusions are physiologically relevant, as NPCs reconstituted in a *Xenopus* egg extract require cohesive FG repeats to maintain their barrier function. Specifically, we show that NPCs lacking Nup98, a nucleoporin with highly cohesive FG repeats, fail to provide a barrier for inert molecules and to actively accumulate NTR•cargo complexes against concentration gradients. The barrier can be restored with Nup98 containing either its own cohesive repeats or even unrelated cohesive repeats. Noncohesive or only partially cohesive FG repeats, even when providing binding sites for NTRs, cannot build a proper barrier. This deficiency cannot be overcome by increasing the concentration of the noncohesive FG domains within the pores. These findings demonstrate that NPC selectivity cannot be explained by NTR•FG interactions alone. Instead, inter-FG cohesion appears to be equally important.

Why Can FG Hydrogels Form an Effective NPC Barrier but Noncohesive FG Brushes Cannot?

The virtual gate model suggested that brushes of noninteracting FG domains are sufficient to exclude inert macromolecules from NPC passage (Rout et al., 2003). The model relates to the fact that brushes (e.g., of PEG chains) can block macromolecules from binding to surfaces. Why then does a multivalently cross-linked FG hydrogel represent a far more efficient NPC barrier? We see several related explanations.

First, a repellence of inert material by noninteracting linear polymers would come down to a volume exclusion effect. Even if one assumes the FG repeats to reach a local concentration of 200 mg/ml, they would exclude only ~1/5 of the available volume. In an FG hydrogel, however, the complete gel volume (comprising also the entrapped solvent) will exclude inert material larger than the mesh size.

Second, one could argue that noncohesive FG domains show an enhanced barrier effect when anchored (as brushes) to a surface. Brushes, however, are effective obstacles only near their anchor points, where Brownian motion cannot displace them. This applies to distances from the grafting surface of no more than a persistence length, which is a measure of the polymer's stiffness. This length is <1 nm for flexible polypeptides (Zhou, 2001) and thus negligibly small compared to the 50-nm-wide central NPC channel or compared to the ~200 nm contour length of a typical FG domain. At greater distances, the grafted chains will not behave as rigid brushes but will behave like freely soluble polymers. As such, FG domains should exert no particular sieving effect and thus constitute no better barrier than other aqueous polymer solutions of the same concentration. Even assuming the local FG domain concentration being as high as 200 mg/ml, inert molecules would diffuse through such a "noncohesive FG cloud" at rates that are not fundamentally different from their diffusion rates in the cytoplasm. In other words, noncohesive FG brushes might hinder inert materials from an encounter with the grafting surface, but they are rather ineffective in suppressing NPC passage, which occurs mostly parallel to and in considerable distance (up to 20 nm) from the grafting surface. In contrast, meshes formed by inter-FG repeat cohesion pose effective barriers independently of any anchoring. This is illustrated by the fact that FG hydrogels can be prepared at macroscopic sizes and yet display NPC-like permeability (Figure 5).

Third, the efficiency of the barrier will increase with the local concentration of FG repeats. This local concentration should depend not only on how much FG mass is anchored but also on the cohesive properties of the repeats. Noncohesive (i.e., highly water-soluble) FG domains will be diluted by entropy effects to a large volume, which further antagonizes barrier formation (see Figure 1 for an illustration). Highly cohesive repeats, in contrast, are poorly water soluble and typically show the opposite behavior, namely a phase separation leading to a very protein-rich phase with strong barrier effects (A.A.L. and D.G., unpublished data). These effects even feed back on the assembly of NPCs in that noncohesive repeats disfavor, whereas cohesive repeats favor, incorporation of Nup98 variants into NPCs (see Figure S6).

(B) Binding of importin-β to selected FG repeats. Equal masses of bacterially expressed FG domains were immobilized on beads and incubated with an excess of importin-β. Importin-β bound to the Nup98 FG domain as well as to the two Nsp1 FG domain fragments, but not to the Φ⇒S mutant of Nup98 FG repeats. Please note that such mutations weaken SDS and Coomassie binding and thereby cause an unusual running behavior on SDS-PAGE and lower staining intensity.
(C) WGA-depleted egg extract was complemented with various Nup98 derivatives and was used for nuclear assembly. See Figure S5 for characterization of the proteins used. NPC incorporation of 3xHA-tagged Nup98 derivatives was confirmed by anti-HA IF. As detailed in Figure S6, Nup98 derivatives with noncohesive repeats required higher concentrations for efficient NPC binding than wild-type Nup98. This inhibition of NPC binding was overcome by fusion to a tetramerizing leucine zipper (LZ). Nup98 chimeras with any type of noncohesive FG repeats were unable to form a barrier against dextran influx into nuclei and to allow nuclear accumulation of the IBB fusion protein.
Scale bars, 25 μm. See also Figure S7.

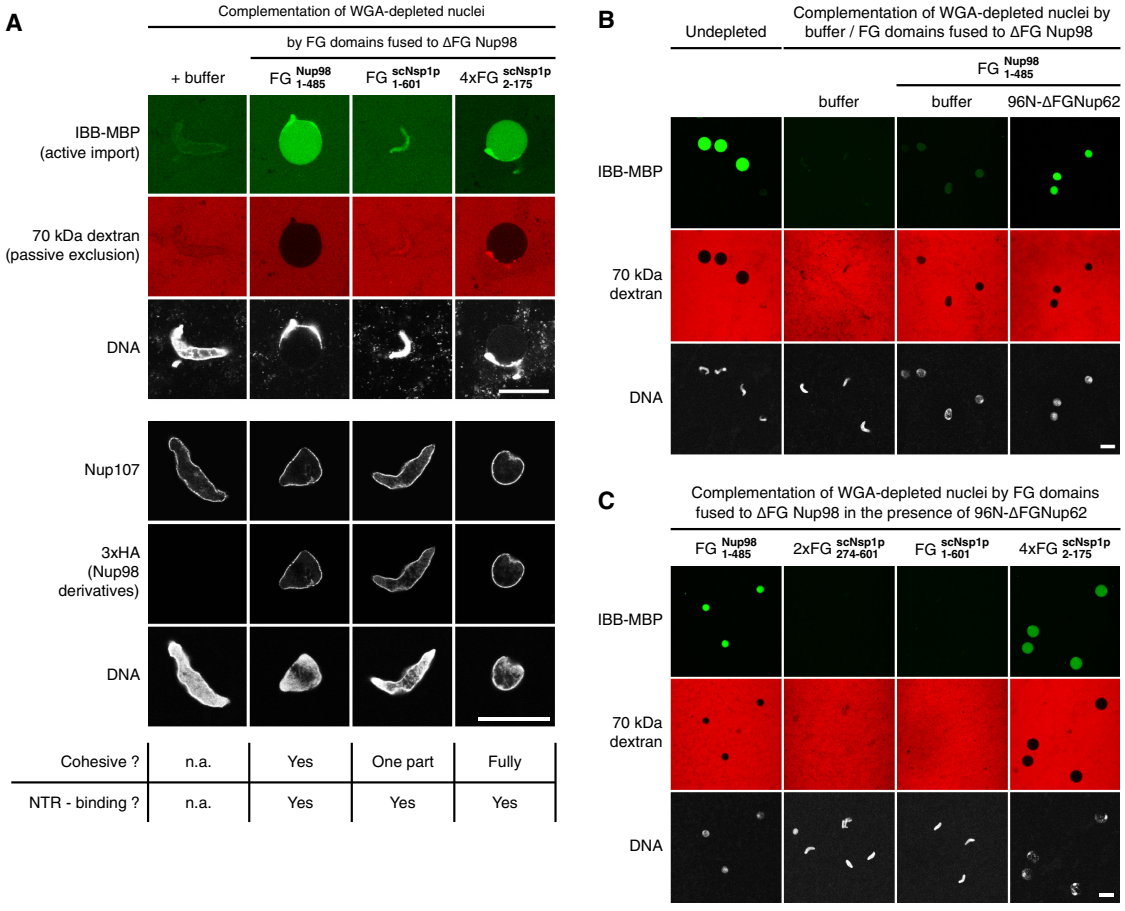
A
Complementation of WGA-depleted nuclei
by FG domains fused to ΔFG Nup98
+ buffer
FG Nup98 1-485
FG scNsp1p 1-601
4xFG scNsp1p 2-175
IBB-MBP (active import)
70 kDa dextran (passive exclusion)
DNA
Nup107
3xHA (Nup98 derivatives)
DNA
Cohesive ?
n.a.
Yes
One part
Fully
NTR - binding ?
n.a.
Yes
Yes
Yes
B
Undepleted
Complementation of WGA-depleted nuclei by buffer / FG domains fused to ΔFG Nup98
FG Nup98 1-485
buffer
buffer
96N-ΔFGNup62
IBB-MBP
70 kDa dextran
DNA
C
Complementation of WGA-depleted nuclei by FG domains fused to ΔFG Nup98 in the presence of 96N-ΔFGNup62
FG Nup98 1-485
2xFG scNsp1p 274-601
FG scNsp1p 1-601
4xFG scNsp1p 2-175
IBB-MBP
70 kDa dextran
DNA
D
NPC channel filled with
FG Nup98 1-485
2xFG scNsp1p 274-601
FG scNsp1p 1-601
4xFG scNsp1p 2-175
COOH
ΔFG Nup98
FG 1-485 cohesive
FG 274-601 non-cohesive
FG 274-601 non-cohesive
FG 2-175 cohesive
FG 2-175 cohesive
NH2
NPC-channel top view
Impβ
inert
cargo
NPC-channel lateral view
Gel

Partially Cohesive FG Domains and the NPC Sealing Problem

One should assume that functional NPCs are organized such that all transiting soluble macromolecules are forced along paths that include at least one region of high selectivity, i.e., a narrow-meshed FG hydrogel. Any leak or path with high nonselective protein conductance would deteriorate the complete barrier system (analogous to an electrical short circuit). Wild-type NPCs of *S. cerevisiae*, however, contain not only highly cohesive FG domains but also Nups with noncohesive subdomains (e.g., Nsp1p, Nup2p, Nup1p, or Nup159p; see Yamada et al., 2010). Why do these noncohesive domains not dominate and render the complete pore nonselective? Apparently, it matters not only what kind of repeats are contained within the central channel but also where and with which topology they are anchored. The FG domain of Nsp1p, which is noncohesive around the anchor point and cohesive only at the distal end, is insufficient for creating a complete barrier, even when anchored at high density (Figure 7). This is probably because this topology creates a thick layer of low selectivity around the anchor points. The FG domains of Nup100 and Nup116, however, appear highly cohesive along their entire sequence. They should thus be able to form barrier layers that control the complete cross-section of the yeast NPC channel, i.e., also those parts that are left leaky by the noncohesive FG domains.

What Is the Function of Noncohesive FG Domains?

Why has *S. cerevisiae* conserved noncohesive FG domains that fail to form a selective NPC barrier on their own? A first explanation is that some FG domains (in particular, the ones found in the peripheral nucleoporins Nup1p, Nup2p, or Nup159p) might primarily function in disassembling import or export complexes (reviewed in Wälde and Kehlenbach, 2010) and not in forming the NPC barrier. Second, noncohesive repeats might modulate the permeability of NPCs. It is clear that a too-leaky barrier cannot maintain nucleocytoplasmic gradients. Too-tight FG hydrogels, however, might also pose a problem when they are not sufficiently permeable for large NTR•cargo complexes. *S. cerevisiae* apparently optimizes the permeability of its NPCs by blending extremely cohesive domains (such as the ones from Nup100p or Nup116p) with less cohesive or even noncohesive ones.

Future Challenges

Even though we can now pinpoint the basic framework for NPC barrier formation, we still miss many of the parameters needed for a description that would be detailed enough to allow, e.g., a faithful computer simulation of the NPC barrier. For example, we do not yet know the minimum length of cohesive FG domains required for basic NPC function, whether it matters which anchor points are used, and whether the great sequence heterogeneity in individual FG repeat units is really required for function. In fact, it is quite possible that block polymers of identical FG repeat units can also form a functional NPC barrier. This would allow a tremendous simplification of barrier complexity. It would pave the way for solving atomic structures of functionally relevant inter-FG contacts and, eventually, for understanding how NTRs transiently disengage those contacts and catalyze their own passage through the barrier. The experimental system presented here will be pivotal for further simplifying NPCs and thus for addressing these questions.

EXPERIMENTAL PROCEDURES

Antibodies

Polyclonal antibodies against *X. laevis* Nup54, Nup62, Nup98, Nup107, and gp210 were newly raised in rabbits. For epitopes, see Extended Experimental Procedures. The monoclonal mouse anti-Nup62 (Cordes et al., 1995) and the rabbit anti-Ndc1 (Stavru et al., 2006) have been described. Guinea pig anti-Nup98 and anti-Nup133 were kind gifts of Volker Cordes. Rabbit anti-HA was from Santa Cruz, and mouse anti-HA and mAB414 were from Covance.

Recombinant Protein Expression

Recombinant proteins were expressed in *E. coli* as detailed in the Extended Experimental Procedures.

Preparation, Depletion, and Use of *X. laevis* Egg Extracts

Detailed protocols are provided in the Extended Experimental Procedures. In short, demembranated sperm chromatin and interphase egg extracts were prepared as described (Blow and Laskey, 1986). Extracts were fractionated into a soluble cytosolic fraction (high-speed supernatant, HSS) and an initial membrane fraction as described (Hetzer et al., 2000). The membrane fraction was further purified by flotation through a layer of 30% iodixanol. HSS was depleted with WGA-Sepharose or immobilized antibodies in up to five consecutive incubations.

A standard 20 μl assembly reaction contained 16 μl HSS, 10 mM creatine phosphate, 0.5 mM ATP, 0.5 mM GTP, 50 μg/ml creatine kinase, and 30,000 demembranated sperm nuclei. In add-back experiments, Nup98 derivatives were typically added to a final concentration of 200 nM. These components were preincubated for 10 min at 18°C before 2 μl membranes (10-fold concentrated as compared to the initial extract) were added.

After 2 hr at 18°C, half of the nuclear assembly reaction was fixed for immunofluorescence. The remaining half was diluted 0.5-fold with buffer containing markers for passive exclusion and active transport, as well as DAPI to visualize DNA. Approximately 1.5 hr later, 1.5 μl of the transport reaction were

Figure 7. An Operational NPC Barrier Requires a Fully Cohesive FG Domain

(A) Indicated Nup98 chimeras were tested at a final concentration of 500 nM for their capacity to create a functional NPC barrier as described in Figure 6. The FG domain from Nsp1p did not yield a functional barrier. It contains an N-terminal cohesive part followed by the already mentioned long noncohesive stretch (274–601) in front of the anchor point. Replacing this noncohesive module by additional copies of the highly cohesive N terminus (4xFG 2–175) allowed formation of a selective NPC barrier. See also Figure S3B.

(B) Complementation of WGA-depleted NPCs by 100 nM Nup98 was studied in the absence or presence of 50 nM 96N-ΔFG Nup54•58•62 complex, which provides additional binding sites ($Nup96^{1-19}$) for Nup98 within the central NPC channel.

(C) Nup98 and its chimeras were added to 500 nM (see Figures 6C and S7), and the 96N-ΔFG Nup62 complex was added to 50 nM. Also, this test with a higher local concentration of FG domains confirmed that a functional NPC barrier requires FG domains that display high cohesiveness from their anchor point over a long sequence.

(D) Scheme for the experiment shown in Figures 6 and 7. For explanation, see main text.

Scale bars, 25 μm.

transferred into a well of a multiwell slide and covered with a coverslip. The nucleocytoplasmic distribution of the fluorescent probes was directly measured by scanning with a confocal microscope through the midplane of the nuclei.

Hydrogel Assay

Nup98 FG repeats were O-GlcNAc modified by incubation with UDP-GlcNAc and the 110 kDa subunit of the human O-GlcNAc transferase (Swiss-Prot, O15294.3; Lubas and Hanover, 2000). Preparation of the FG hydrogel and the gel permeation assay were essentially as described before (Frey and Görlich, 2009).

ACCESSION NUMBERS

The complete coding sequence of *Xenopus tropicalis* Nup98-Nup96 was given the accession number JX136847 (available from GenBank/EMBL/DDBJ).

SUPPLEMENTAL INFORMATION

Supplemental Information includes Extended Experimental Procedures and seven figures and can be found with this article online at http://dx.doi.org/10.1016/j.cell.2012.07.019.

ACKNOWLEDGMENTS

We wish to thank S. Frey for sharing vectors and expertise; H. Behr, R. Rees, H.-J. Dehne, and J. Krull for excellent technical help; W.W. Franke and V.C. Cordes for the CO2-225 monoclonal anti-Nup62 cell line; V.C. Cordes for guinea pig anti-Nup98 and Nup133; D. van Aalten for the NagJ expression construct; T.A. Rapoport for stimulating discussion on the manuscript; and V.C. Cordes, S. Frey, K. Kirli, and M. Samwer for critical reading.

Received: February 24, 2012
Revised: April 5, 2012
Accepted: June 5, 2012
Published: August 16, 2012

REFERENCES

Ader, C., Frey, S., Maas, W., Schmidt, H.B., Görlich, D., and Baldus, M. (2010). Amyloid-like interactions within nucleoporin FG hydrogels. Proc. Natl. Acad. Sci. USA *107*, 6281–6285.

Bayliss, R., Ribbeck, K., Akin, D., Kent, H.M., Feldherr, C.M., Görlich, D., and Stewart, M. (1999). Interaction between NTF2 and xFxFG-containing nucleoporins is required to mediate nuclear import of RanGDP. J. Mol. Biol. *293*, 579–593.

Bayliss, R., Littlewood, T., and Stewart, M. (2000). Structural basis for the interaction between FxFG nucleoporin repeats and importin-beta in nuclear trafficking. Cell *102*, 99–108.

Belgareh, N., Rabut, G., Baï, S.W., van Overbeek, M., Beaudouin, J., Daigle, N., Zatsepina, O.V., Pasteau, F., Labas, V., Fromont-Racine, M., et al. (2001). An evolutionarily conserved NPC subcomplex, which redistributes in part to kinetochores in mammalian cells. J. Cell Biol. *154*, 1147–1160.

Blow, J.J., and Laskey, R.A. (1986). Initiation of DNA replication in nuclei and purified DNA by a cell-free extract of Xenopus eggs. Cell *47*, 577–587.

Brohawn, S.G., Partridge, J.R., Whittle, J.R., and Schwartz, T.U. (2009). The nuclear pore complex has entered the atomic age. Structure *17*, 1156–1168.

Clarkson, W.D., Kent, H.M., and Stewart, M. (1996). Separate binding sites on nuclear transport factor 2 (NTF2) for GDP-Ran and the phenylalanine-rich repeat regions of nucleoporins p62 and Nsp1p. J. Mol. Biol. *263*, 517–524.

Cordes, V.C., Reidenbach, S., and Franke, W.W. (1995). High content of a nuclear pore complex protein in cytoplasmic annulate lamellae of Xenopus oocytes. Eur. J. Cell Biol. *68*, 240–255.

Cronshaw, J.M., Krutchinsky, A.N., Zhang, W., Chait, B.T., and Matunis, M.J. (2002). Proteomic analysis of the mammalian nuclear pore complex. J. Cell Biol. *158*, 915–927.

Denning, D.P., Patel, S.S., Uversky, V., Fink, A.L., and Rexach, M. (2003). Disorder in the nuclear pore complex: the FG repeat regions of nucleoporins are natively unfolded. Proc. Natl. Acad. Sci. USA *100*, 2450–2455.

Finlay, D.R., and Forbes, D.J. (1990). Reconstitution of biochemically altered nuclear pores: transport can be eliminated and restored. Cell *60*, 17–29.

Finlay, D.R., Meier, E., Bradley, P., Horecka, J., and Forbes, D.J. (1991). A complex of nuclear pore proteins required for pore function. J. Cell Biol. *114*, 169–183.

Forbes, D.J., Kirschner, M.W., and Newport, J.W. (1983). Spontaneous formation of nucleus-like structures around bacteriophage DNA microinjected into Xenopus eggs. Cell *34*, 13–23.

Fornerod, M., van Deursen, J., van Baal, S., Reynolds, A., Davis, D., Murti, K.G., Fransen, J., and Grosveld, G. (1997). The human homologue of yeast CRM1 is in a dynamic subcomplex with CAN/Nup214 and a novel nuclear pore component Nup88. EMBO J. *16*, 807–816.

Frey, S., and Görlich, D. (2007). A saturated FG-repeat hydrogel can reproduce the permeability properties of nuclear pore complexes. Cell *130*, 512–523.

Frey, S., and Görlich, D. (2009). FG/FxFG as well as GLFG repeats form a selective permeability barrier with self-healing properties. EMBO J. *28*, 2554–2567.

Frey, S., Richter, R.P., and Görlich, D. (2006). FG-rich repeats of nuclear pore proteins form a three-dimensional meshwork with hydrogel-like properties. Science *314*, 815–817.

Görlich, D., and Kutay, U. (1999). Transport between the cell nucleus and the cytoplasm. Annu. Rev. Cell Dev. Biol. *15*, 607–660.

Görlich, D., Henklein, P., Laskey, R., and Hartmann, E. (1996). A 41 amino acid motif in importin alpha confers binding to importin beta and hence transit into the nucleus. EMBO J. *15*, 1810–1817.

Görlich, D., Seewald, M.J., and Ribbeck, K. (2003). Characterization of Ran-driven cargo transport and the RanGTPase system by kinetic measurements and computer simulation. EMBO J. *22*, 1088–1100.

Griffis, E.R., Xu, S., and Powers, M.A. (2003). Nup98 localizes to both nuclear and cytoplasmic sides of the nuclear pore and binds to two distinct nucleoporin subcomplexes. Mol. Biol. Cell *14*, 600–610.

Grote, M., Kubitscheck, U., Reichelt, R., and Peters, R. (1995). Mapping of nucleoporins to the center of the nuclear pore complex by post-embedding immunogold electron microscopy. J. Cell Sci. *108*, 2963–2972.

Harbury, P.B., Zhang, T., Kim, P.S., and Alber, T. (1993). A switch between two-, three-, and four-stranded coiled coils in GCN4 leucine zipper mutants. Science *262*, 1401–1407.

Hetzer, M.W., and Wente, S.R. (2009). Border control at the nucleus: biogenesis and organization of the nuclear membrane and pore complexes. Dev. Cell *17*, 606–616.

Hetzer, M., Bilbao-Cortés, D., Walther, T.C., Gruss, O.J., and Mattaj, I.W. (2000). GTP hydrolysis by Ran is required for nuclear envelope assembly. Mol. Cell *5*, 1013–1024.

Hodel, A.E., Hodel, M.R., Griffis, E.R., Hennig, K.A., Ratner, G.A., Xu, S., and Powers, M.A. (2002). The three-dimensional structure of the autoproteolytic, nuclear pore-targeting domain of the human nucleoporin Nup98. Mol. Cell *10*, 347–358.

Hu, T., Guan, T., and Gerace, L. (1996). Molecular and functional characterization of the p62 complex, an assembly of nuclear pore complex glycoproteins. J. Cell Biol. *134*, 589–601.

Hurt, E.C. (1988). A novel nucleoskeletal-like protein located at the nuclear periphery is required for the life cycle of Saccharomyces cerevisiae. EMBO J. *7*, 4323–4334.

Iovine, M.K., Watkins, J.L., and Wente, S.R. (1995). The GLFG repetitive region of the nucleoporin Nup116p interacts with Kap95p, an essential yeast nuclear import factor. J. Cell Biol. *131*, 1699–1713.

Isgro, T.A., and Schulten, K. (2005). Binding dynamics of isolated nucleoporin repeat regions to importin-β. Structure *13*, 1869–1879.

Krull, S., Thyberg, J., Björkroth, B., Rackwitz, H.R., and Cordes, V.C. (2004). Nucleoporins as components of the nuclear pore complex core structure

and Tpr as the architectural element of the nuclear basket. Mol. Biol. Cell *15*, 4261–4277.

Kubitscheck, U., Grünwald, D., Hoekstra, A., Rohleder, D., Kues, T., Siebrasse, J.P., and Peters, R. (2005). Nuclear transport of single molecules: dwell times at the nuclear pore complex. J. Cell Biol. *168*, 233–243.

Kustanovich, T., and Rabin, Y. (2004). Metastable network model of protein transport through nuclear pores. Biophys. J. *86*, 2008–2016.

Laurell, E., Beck, K., Krupina, K., Theerthagiri, G., Bodenmiller, B., Horvath, P., Aebersold, R., Antonin, W., and Kutay, U. (2011). Phosphorylation of Nup98 by multiple kinases is crucial for NPC disassembly during mitotic entry. Cell *144*, 539–550.

Li, S.J., and Hochstrasser, M. (1999). A new protease required for cell-cycle progression in yeast. Nature *398*, 246–251.

Lim, R.Y., Fahrenkrog, B., Köser, J., Schwarz-Herion, K., Deng, J., and Aebi, U. (2007). Nanomechanical basis of selective gating by the nuclear pore complex. Science *318*, 640–643.

Lohka, M.J., and Masui, Y. (1983). Formation in vitro of sperm pronuclei and mitotic chromosomes induced by amphibian ooplasmic components. Science *220*, 719–721.

Lowe, A.R., Siegel, J.J., Kalab, P., Siu, M., Weis, K., and Liphardt, J.T. (2010). Selectivity mechanism of the nuclear pore complex characterized by single cargo tracking. Nature *467*, 600–603.

Lu, Z.H., Sittman, D.B., Brown, D.T., Munshi, R., and Leno, G.H. (1997). Histone H1 modulates DNA replication through multiple pathways in Xenopus egg extract. J. Cell Sci. *110*, 2745–2758.

Lubas, W.A., and Hanover, J.A. (2000). Functional expression of O-linked GlcNAc transferase. Domain structure and substrate specificity. J. Biol. Chem. *275*, 10983–10988.

Macaulay, C., Meier, E., and Forbes, D.J. (1995). Differential mitotic phosphorylation of proteins of the nuclear pore complex. J. Biol. Chem. *270*, 254–262.

Milles, S., and Lemke, E.A. (2011). Single molecule study of the intrinsically disordered FG-repeat nucleoporin 153. Biophys. J. *101*, 1710–1719.

Mohr, D., Frey, S., Fischer, T., Güttler, T., and Görlich, D. (2009). Characterisation of the passive permeability barrier of nuclear pore complexes. EMBO J. *28*, 2541–2553.

Panté, N., and Kann, M. (2002). Nuclear pore complex is able to transport macromolecules with diameters of about 39 nm. Mol. Biol. Cell *13*, 425–434.

Patel, S.S., Belmont, B.J., Sante, J.M., and Rexach, M.F. (2007). Natively unfolded nucleoporins gate protein diffusion across the nuclear pore complex. Cell *129*, 83–96.

Peters, R. (2005). Translocation through the nuclear pore complex: selectivity and speed by reduction-of-dimensionality. Traffic *6*, 421–427.

Powers, M.A., Macaulay, C., Masiarz, F.R., and Forbes, D.J. (1995). Reconstituted nuclei depleted of a vertebrate GLFG nuclear pore protein, p97, import but are defective in nuclear growth and replication. J. Cell Biol. *128*, 721–736.

Radu, A., Moore, M.S., and Blobel, G. (1995). The peptide repeat domain of nucleoporin Nup98 functions as a docking site in transport across the nuclear pore complex. Cell *81*, 215–222.

Rao, F.V., Dorfmueller, H.C., Villa, F., Allwood, M., Eggleston, I.M., and van Aalten, D.M. (2006). Structural insights into the mechanism and inhibition of eukaryotic O-GlcNAc hydrolysis. EMBO J. *25*, 1569–1578.

Rexach, M., and Blobel, G. (1995). Protein import into nuclei: association and dissociation reactions involving transport substrate, transport factors, and nucleoporins. Cell *83*, 683–692.

Ribbeck, K., and Görlich, D. (2001). Kinetic analysis of translocation through nuclear pore complexes. EMBO J. *20*, 1320–1330.

Rout, M.P., Aitchison, J.D., Magnasco, M.O., and Chait, B.T. (2003). Virtual gating and nuclear transport: the hole picture. Trends Cell Biol. *13*, 622–628.

Schrader, N., Stelter, P., Flemming, D., Kunze, R., Hurt, E., and Vetter, I.R. (2008). Structural basis of the nic96 subcomplex organization in the nuclear pore channel. Mol. Cell *29*, 46–55.

Stavru, F., Hülsmann, B.B., Spang, A., Hartmann, E., Cordes, V.C., and Görlich, D. (2006). NDC1: a crucial membrane-integral nucleoporin of metazoan nuclear pore complexes. J. Cell Biol. *173*, 509–519.

Strawn, L.A., Shen, T., Shulga, N., Goldfarb, D.S., and Wente, S.R. (2004). Minimal nuclear pore complexes define FG repeat domains essential for transport. Nat. Cell Biol. *6*, 197–206.

Terry, L.J., and Wente, S.R. (2009). Flexible gates: dynamic topologies and functions for FG nucleoporins in nucleocytoplasmic transport. Eukaryot. Cell *8*, 1814–1827.

Tu, L.C., and Musser, S.M. (2011). Single molecule studies of nucleocytoplasmic transport. Biochim. Biophys. Acta *1813*, 1607–1618.

Vasu, S., Shah, S., Orjalo, A., Park, M., Fischer, W.H., and Forbes, D.J. (2001). Novel vertebrate nucleoporins Nup133 and Nup160 play a role in mRNA export. J. Cell Biol. *155*, 339–354.

Wälde, S., and Kehlenbach, R.H. (2010). The part and the whole: functions of nucleoporins in nucleocytoplasmic transport. Trends Cell Biol. *20*, 461–469.

Watson, M.L. (1954). Pores in the mammalian nuclear membrane. Biochim. Biophys. Acta *15*, 475–479.

Weis, K. (2007). The nuclear pore complex: oily spaghetti or gummy bear? Cell *130*, 405–407.

Wente, S.R., Rout, M.P., and Blobel, G. (1992). A new family of yeast nuclear pore complex proteins. J. Cell Biol. *119*, 705–723.

Yamada, J., Phillips, J.L., Patel, S., Goldfien, G., Calestagne-Morelli, A., Huang, H., Reza, R., Acheson, J., Krishnan, V.V., Newsam, S., et al. (2010). A bimodal distribution of two distinct categories of intrinsically disordered structures with separate functions in FG nucleoporins. Mol. Cell. Proteomics *9*, 2205–2224.

Yang, W., Gelles, J., and Musser, S.M. (2004). Imaging of single-molecule translocation through nuclear pore complexes. Proc. Natl. Acad. Sci. USA *101*, 12887–12892.

Zhou, H.-X. (2001). Loops in proteins can be modeled as worm-like chains. J. Phys. Chem. B *105*, 6763–6766.

Cell

EXTENDED EXPERIMENTAL PROCEDURES

Generation of Polyclonal Rabbit Antibodies against *Xenopus* Nucleoporins

Antibodies were raised in rabbits against the extreme C-termini of *Xenopus* Nup54 (UniProtKB: Q6PAY1, residues 488-502) and Nup62 (UniProtKB: Q91349, residues 533-547), against ΔFG Nup98 (corresponding to residues 486-866 of the complete *X. tropicalis* sequence) and against residues 2-100 of Nup107 (UniProtKB: A2RV69). Anti-gp210 was raised against the C terminus of gp210 (residues 184-240 of accession AAV98364; Antonin et al., 2005).

A crucial criterion for the choice of epitopes was that the resulting antibodies recognize all so far discernable isoforms of their respective target proteins. All antibodies were affinity purified on immobilized antigens and subsequently tested for potential cross-reactions against other *Xenopus laevis* proteins by immunoblotting (see e.g., Figure S1A).

Quantitative Immunoblotting

Protein mixtures were separated by SDS-PAGE and transferred onto a nitrocellulose membrane. After blocking, the membrane was consecutively incubated with primary antibodies at a final concentration of 1 μg/ml and IRDye secondary antibodies (LI-COR Biosciences) used at a 1:5 000 dilution, and analyzed with an Odyssey Infrared Imaging System (LI-COR Biosciences). Quantification was by integration of fluorescent signals in ImageJ. Infrared imaging has the advantage over chemiluminescence detection that the signal of bound secondary antibodies is linear over 3-4 orders of magnitude.

The blots shown in Figures 2A, 3A, and 3D contained 1 μl HSS per lane, i.e., the amount of egg cytosol present in 1.25 μl nuclear assembly reaction. In Figure 2A, the amounts of membranes and chromatin loaded correspond to the equivalent of 2.5 μl nuclear assembly reaction. For even higher sensitivity the amount of membranes analyzed in Figure S1D corresponds to the equivalent of a 10 μl nuclear assembly reaction.

The absolute concentration of endogenous Nup98 in undepleted extracts was determined by comparative immunoblotting. Bacterially expressed His_{14}-tagged full length *Xenopus* Nup98 purified under denaturing conditions to homogeneity served as a standard. Its concentration was determined photometrically at 280 nm, assuming a molar absorptivity of 32 200 $M^{-1} \cdot cm$.

To quantify Nup98 chimeras prior to add-back experiments, we spotted the purified proteins onto nitrocelluose using a Bio-Dot microfiltration apparatus (Bio-Rad), and detected them by infrared-imaging using antibodies against ΔFG Nup98 ($Nup98^{488–866}$) and IR-dye labeled secondary antibodies. Because the proteins had been purified through N-terminal His-tags and detected through a C-terminal epitope, this quantitation procedure excludes truncation products that would not be incorporated into NPCs.

Cytosolic Fractions, Membranes, and Chromatin for Nuclear Assembly Reactions

We adapted and optimized published protocols to maximize the robustness of the system and to minimize residual levels of Nup98 and Nup62 in depleted extracts.

Demembranated sperm chromatin was prepared as described (Blow and Laskey, 1986). Special care was taken to avoid any contamination with somatic nuclei. As a result, the Nup contamination of the final preparation was below the detection limit (Figure 2A; data not shown).

HKMS (20 mM HEPES/KOH pH 7.5, 90 mM KOAc, 2 mM MgOAc, 250 mM sucrose) was the basic buffer for nuclear assembly, used for diluting extracts and components, resuspending membranes, equilibrating beads etc. Low speed interphase extracts from Ca^{2+}-ionophore activated *Xenopus laevis* eggs (LSS) were prepared and supplemented with cycloheximide as described (Blow and Laskey, 1986). The LSS was further fractionated as described (Hetzer et al., 2000) into a soluble cytosolic fraction (high speed supernatant, HSS) and an assembly-competent membrane fraction. To remove traces of soluble nucleoporins from the initial membrane fraction, it was further purified by flotation through a layer of 30% iodixanol (OptiPrep Density Gradient Medium, Sigma) in HKMS.

Depletion of *Xenopus* Egg Extracts

Depletions were carried out with either WGA-Sepharose CL-4B (Fluka) or antibodies immobilized on superparamagnetic beads. Rabbit IgGs (anti-Nup54, anti-Nup62, anti-Nup98 as well as anti-GFP that served as mock antibodies) were pre-bound to Dynabeads Protein A (Invitrogen) at ≈10 μg IgG per mg of beads, and covalently linked with 0.02% w/v glutaraldehyde, followed by quenching with glycine and reduction of Schiff bases with 3 mg/ml sodium cyanoborohydride. Mouse monoclonal anti-Nup62 IgGs were immobilized the same way to Dynabeads Protein G (Invitrogen). Specificity of the beads was validated by immunoprecipitation analysis (Figures S1B and S1C).

Full depletions required three to five consecutive incubations, each performed for 1h at 4°C with gentle head-over-head mixing. After each round, beads were collected and the supernatant was transferred onto another aliquot of fresh beads. Mock depletion experiments consistently validated that extracts tolerated at least 6 rounds of depletion without any detectable loss in nuclear assembly activity. Complete depletion of 1 ml freshly prepared HSS required a total of 500-700 μg immobilized IgG or 480 μl of (spin-dried) WGA-Sepharose. For Nup62 depletion, we used a combination of rabbit anti-Nup62 and mouse anti-Nup62. Immunoblot analyses of the depletions are shown in Figures 2A and 3A.

Increasing the stringency of WGA depletion did not further reduce the residual level of Nup62 (data not shown). The remaining band appears downshifted compared to the bulk Nup62 (Figure 2A, lane 12, top Nup62 panel). Apparently, it is not fully O-GlcNAc-modified, which would explain why it did not bind to WGA but remained in the extract.

Nuclear Assembly and Transport Assays

A standard 20 μl assembly reaction contained 16 μl HSS, 1 μl of a 20x energy regenerating system (20 mM HEPES/KOH pH 7.5, 200 mM creatine phosphate, 10 mM ATP, 10 mM GTP, 1 mg/ml creatine kinase and 250 mM sucrose), 1 μl sperm chromatin (with 30 000 demembranated sperms/μl). These components were pre-incubated at 18°C to allow initial decondensation of sperm chromatin (Lohka and Masui, 1984). 2 μl membranes (10-fold concentrated as compared to an LSS) were added 10 min later, and the mixture was incubated for another 2h. In add-back experiments, 1 μl of cytosol was replaced by either HKMS (buffer control) or by the indicated Nup98 derivative prediluted in HKMS. Unless stated otherwise, final concentration of Nup98 variants was 200 nM matching the concentration of endogenous Nup98 in non-depleted HSS (this study).

For analysis, nuclear assembly reactions were split. 10 μl were directly fixed for immunofluorescence (see below). The remaining 10 μl were diluted with 5 μl HKMS, containing markers for passive exclusion and active transport as well as DAPI to visualize DNA. ≈1.5 hr later, 1.5 μl of the transport reaction were transferred into a well of a multiwell slide (MP Biomedicals, Cat. No. 6110009) and sealed with a coverslip. The nucleocytoplasmic distribution of the fluorescent probes was measured by scanning with a confocal microscope (Leica TCS SP5) through the midplane of the nuclei. DAPI-staining of DNA served to unambiguously localize all in vitro assembled nuclei, including those that lacked a permeability barrier. Please note that the quality of egg extracts used allowed functional analysis of nuclei as late as 6 hr after initiating nuclear assembly, even when the extract had suffered a lengthy depletion procedure to remove Nup62-containing complexes.

In detail, the functional assay performed for Figure 2D finally contained 0.5 μM Alexa Fluor 647 labeled IBB-MBP, 0.2 mg/ml 70 kDa Rhodamin-Dextrane (Molecular Probes), 0.8 μM NES-GFP, 0.5 μM exogenous CRM1 and 1 μg/ml DAPI. GFP carrying a non-functional NES mutant equilibrated between nucleus and cytosol within 15 min (data not shown). Thus, the stable exclusion of NES depended on active, CRM1-dependent transport. All other experiments shown were performed with 3 μM Alexa Fluor 568 labeled IBB-MBP, 0.2 mg/ml 70 kDa FITC labeled dextran (Invitrogen) and 1 μg/ml DAPI. For clarity, we display exclusion of inert molecules in red, active nuclear export in cyan, active nuclear import in green and DNA in gray.

Immunofluorescence

Assembled nuclei were fixed by the addition of 0.5 ml 2.4% w/v paraformaldehyde in PBS containing 100 mM sucrose and centrifuged through a cushion made from 30% w/v sucrose in PBS onto (3-aminopropyl) trimethoxysilane-coated coverslips. After blocking with BSA and goat serum, coverslips were incubated with primary antibodies at a final dilution of 5 μg/ml. Alexa Fluor Dye conjugated secondary goat antibodies (Invitrogen) were cross-absorbed with beads containing non-cognate IgGs and used at 1:500 dilution. DAPI was used at 0.2 μg/ml. Coverslips were mounted in VECTASHIELD Mounting medium (Vector Laboratories) and images were recorded using a confocal laser scanning microscope (Leica TCS SP5).

Quantification of Nuclear Rim Signal

ImageJ and Microsoft Excel were used for generation of the line profile (Figure 2C) as well as for quantification of NPC incorporated Nup62 (data not shown).

In detail, for quantification of the Nup62 signal at the nuclear rim, regions of interest were defined by the signal from the Nup107 channel. Signal intensities were then integrated separately for both channels, whereby a baseline correction was applied. The Nup62 signals were then normalized to the NPC density represented by Nup107 staining. This quantitation revealed that the anti-Nup62 depletion reduced the Nup62 signal at the nuclear rim at least 100-fold (data not shown).

Binding of Importin-β to Selected FG Repeats

30 μg of bacterially expressed FG repeat domains were immobilized on Ni(II) beads via N-terminal His_{14}-tags. The beads were then incubated in a total volume of 100 μl with 4 μM importin-β, 50 mM Tris/HCl pH 7.5, 200 mM NaCl, 2 mM $MgCl_2$, 2 mM DTT. Beads were washed and bound importin-β was eluted with 5% SDS, which disrupts protein-protein interactions, but not the binding of the His_{14}-tag to the Ni(II) beads. Subsequently, bait proteins were eluted with sample buffer supplemented with 0.5 M imidazole. Eluate fractions were analyzed by SDS-PAGE and Coomassie Blue staining.

Recombinant Protein Expression

All recombinant proteins were expressed at 18°C for 2 hr in *E. coli* with N-terminal oligo histidine tags and purified by IMAC on a Ni(II) chelate matrix based on PEG-passivated Silica with 1,000 Å pores. Proteins were loaded in 50 mM Tris/HCl pH 7.5, 500 mM NaCl, 20 mM imidazole, 10 mM DTT, and eluted with 1M imidazole pH 7.5. Exchange to imidazole-free buffers (50 mM Tris/HCl pH 7.5, 500 NaCl, 250 mM sucrose, 2 mM DTT) was on Sephadex G25 columns. Maps of the used DNA constructs and more detailed protocols for protein expression are available on request.

To obtain an immunoblotting standard, full length Nup98 was expressed only with a His_{14}-tag and purified from inclusion bodies by IMAC in the presence of 6 M guanidinium hydrochloride.

The import substrates IBB-MBP (labeled with Alexa Fluor 568 or Alexa Fluor 647), the fusion between GFP and wild-type PKI NES, and the expression of CRM1 have been described before (Ribbeck and Görlich, 2002; Güttler et al., 2010). Human importin-β was expressed with and purified via an N-terminal oligo histidine tag.

The ΔFG Nup54•58•62 complex and 96N-ΔFG Nup54•58•62 complex were prepared by coexpression in *E. coli*. A His_{14}-MBP-SUMO-tag on the N-terminus of its Nup62 / 96N-Nup62 subunit allowed purification by Ni(II) chelate chromatography. The complex was subsequently immobilized on IgG sepharose via a zz-SUMO-tag fused to the N-terminus of ΔFG Nup54. The complex was finally eluted by cleavage with SUMO-protease. This also removed the His_{14}-MBP-SUMO-tag from the 96N-Nup62 module such that an authentic Nup96 N-terminus was generated (Fontoura et al., 1999; Hodel et al., 2002; Ratner et al., 2007).

SUPPLEMENTAL REFERENCES

Antonin, W., Franz, C., Haselmann, U., Antony, C., and Mattaj, I.W. (2005). The integral membrane nucleoporin pom121 functionally links nuclear pore complex assembly and nuclear envelope formation. Mol. Cell *17*, 83–92.

Fontoura, B.M., Blobel, G., and Matunis, M.J. (1999). A conserved biogenesis pathway for nucleoporins: proteolytic processing of a 186-kilodalton precursor generates Nup98 and the novel nucleoporin, Nup96. J. Cell Biol. *144*, 1097–1112.

Grandi, P., Dang, T., Pané, N., Shevchenko, A., Mann, M., Forbes, D.J., and Hurt, E.C. (1997). Nup93, a vertebrate homologue of yeast Nic96p, forms a complex with a novel 205-kDa protein and is required for correct nuclear pore assembly. Mol. Biol. Cell *8*, 2017–2038.

Güttler, T., Madl, T., Neumann, P., Deichsel, D., Corsini, L., Monecke, T., Ficner, R., Sattler, M., and Görlich, D. (2010). NES consensus redefined by structures of PKI-type and Rev-type nuclear export signals bound to CRM1. Nat. Struct. Mol. Biol. *17*, 1367–1376.

Lohka, M.J., and Masui, Y. (1984). Roles of cytosol and cytoplasmic particles in nuclear envelope assembly and sperm pronuclear formation in cell-free preparations from amphibian eggs. J. Cell Biol. *98*, 1222–1230.

Meier, E., Miller, B.R., and Forbes, D.J. (1995). Nuclear pore complex assembly studied with a biochemical assay for annulate lamellae formation. J. Cell Biol. *129*, 1459–1472.

Miller, B.R., Powers, M., Park, M., Fischer, W., and Forbes, D.J. (2000). Identification of a new vertebrate nucleoporin, Nup188, with the use of a novel organelle trap assay. Mol. Biol. Cell *11*, 3381–3396.

Ratner, G.A., Hodel, A.E., and Powers, M.A. (2007). Molecular determinants of binding between Gly-Leu-Phe-Gly nucleoporins and the nuclear pore complex. J. Biol. Chem. *282*, 33968–33976.

Ribbeck, K., and Görlich, D. (2002). The permeability barrier of nuclear pore complexes appears to operate via hydrophobic exclusion. EMBO J. *21*, 2664–2671.

Sachdev, R., Sieverding, C., Flotenmeyer, M., and Antonin, W. (2012). The C-terminal domain of Nup93 is essential for assembly of the structural backbone of nuclear pore complexes. Mol. Biol. Cell *23*, 740–749.

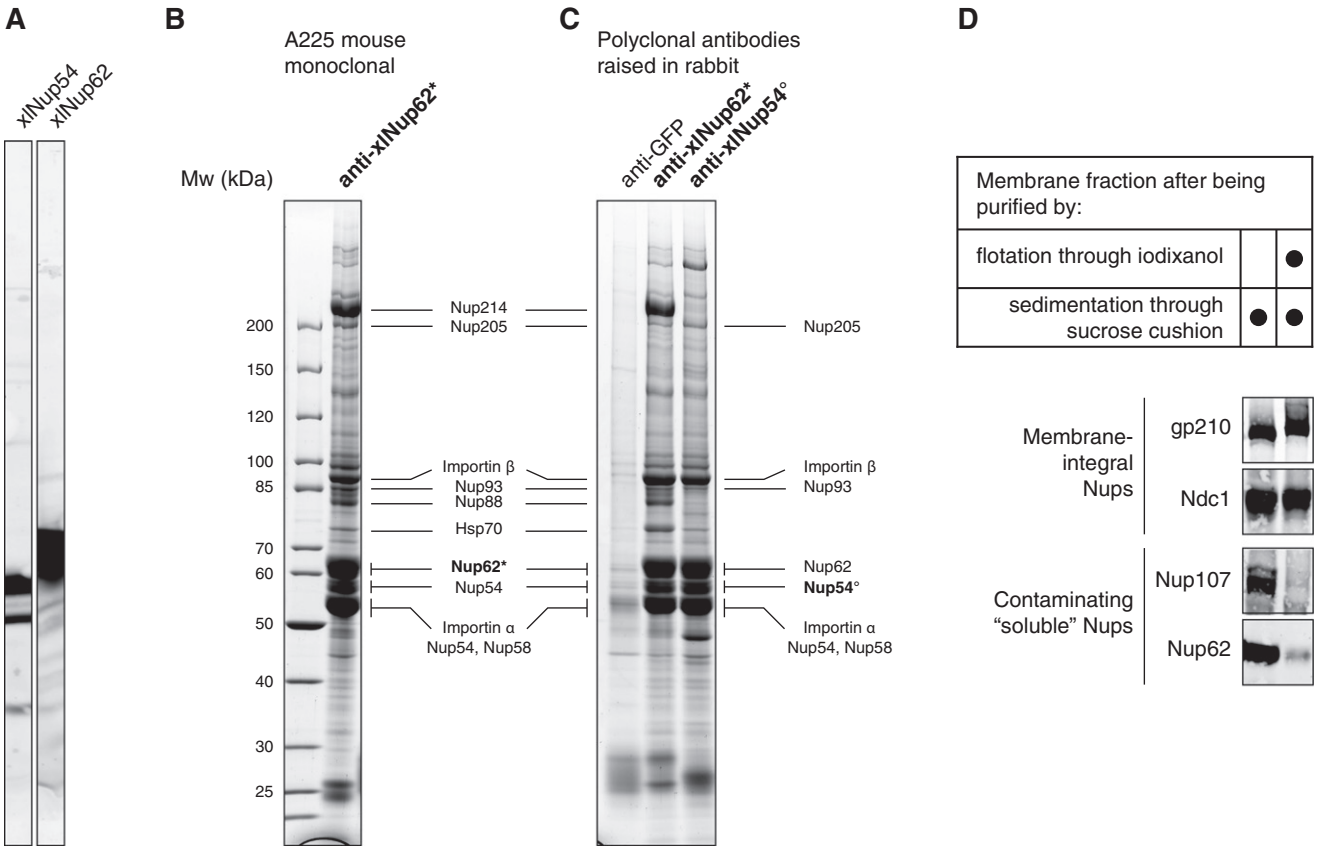

Figure S1. Characterization of Antibodies Used for Depletion of Nup62 Complexes and Purification of Membranes by Flotation, Related to Figure 2A

(A) Rabbit polyclonal antibodies were tested on nitrocellulose stripes containing SDS-PAGE-separated proteins from *X. laevis* egg extract (LSS). The multiple Nup54 reactive bands represent distinct isoforms expressed in *X. laevis* (not shown). The fuzzy appearance of the Nup62 band is due to heterogeneous O-GlcNAc-modification (see also Figures 2A and 3D).

(B and C) Immobilized antibodies against Nup54 and Nup62 were used to immunoprecipitate proteins from *X. laevis* egg extract. SDS-eluted proteins were separated by SDS-PAGE and stained with Coomassie. Indicated bands were identified by mass spectrometry. (B) The monoclonal anti-Nup62 retrieved both, the Nup54•58•62 and Nup62•88•214 complex, along with substoichiometric amounts of Nup93 and Nup205, which anchor these complexes to the NPC scaffold (Grandi et al., 1997; Miller et al., 2000; Sachdev et al., 2012). (C) Polyclonal anti-Nup62 retrieved a virtually identical protein pattern as the mouse monoclonal. Given that both antibodies recognize distinct epitopes such similarity demonstrates a high specificity. Anti-Nup54 recognized the Nup54•58•62 but not the Nup62•88•214 complex.

(D) The immunoblot analysis compares different methods of isolating membranes from *X. laevis* egg extract (LSS). When re-combined with cytosol, traditionally purified membranes contribute Nup62 to a concentration that equals 1%–2% of the source extract. This undermined our efforts to generate NPCs lacking Nup62. Such contamination probably originates from annulate lamellae (AL; Cordes et al., 1995; Meier et al., 1995). It could be removed by a flotation step, exploiting the higher density of AL compared to assembly-competent membranes (Meier et al., 1995). Among all density media tested iodixanol performed best. Flotation-purified membranes were used for all nuclear assembly experiments.

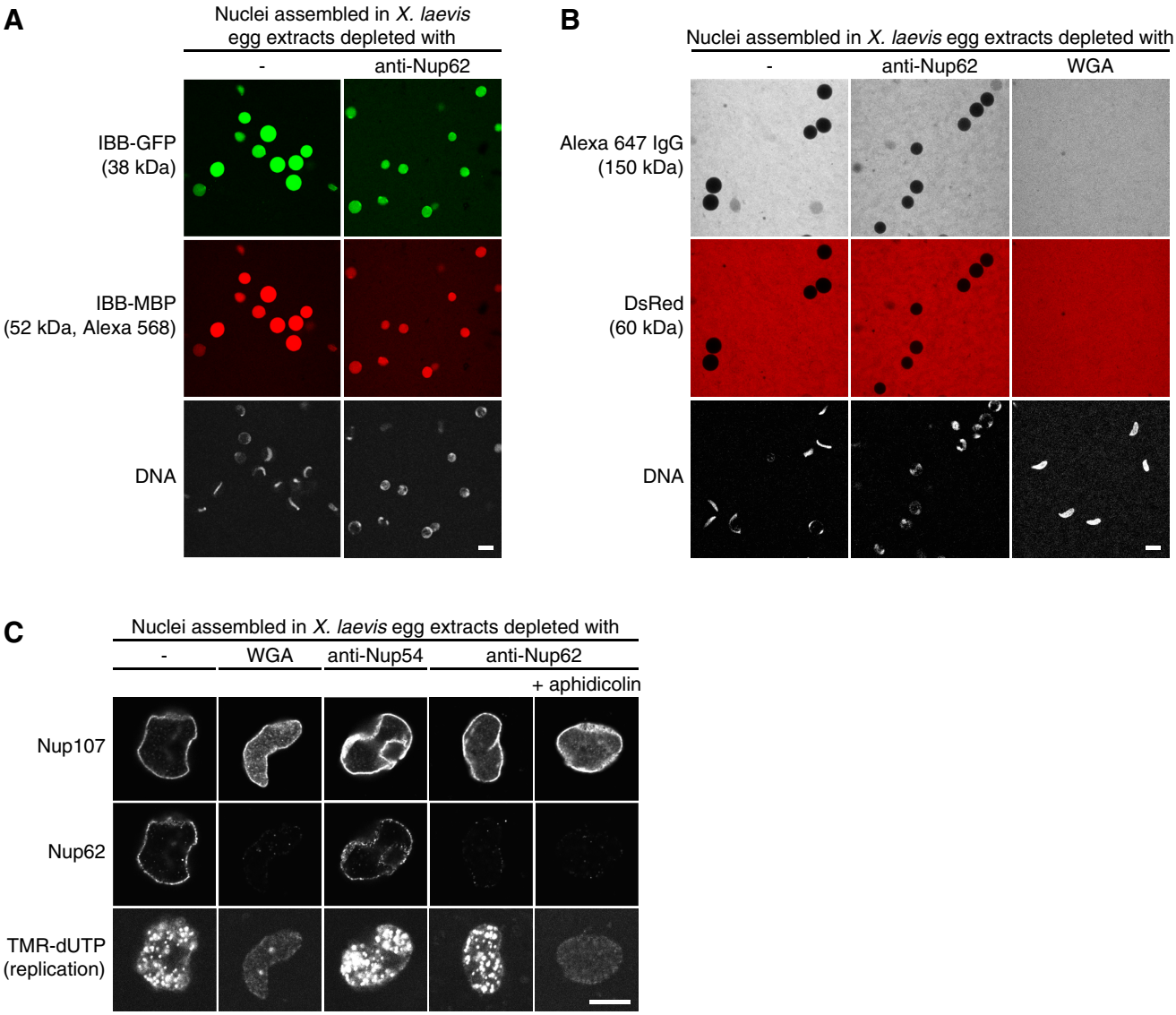

Figure S2. Nuclei Assembled in Nup62-Depleted Extract Display Unexpectedly Mild Functional Defects, Related to Figure 2D

Nuclei were assembled from *Xenopus* sperm chromatin, membranes and undepleted or depleted extracts as indicated. Nucleocytoplasmic distributions of fluorescent permeation probes were recorded by confocal scans through unfixed transport reactions. Scale bars, 25 μm.

(A) Nup62-depleted nuclei display active nuclear import. The fluorescent cargos IBB-GFP and Alexa 568 IBB-MBP were added after nuclear assembly. As both proteins behaved identically, only fluorescently labeled IBB-MBP was used in subsequent experiments.

(B) WGA-deleted nuclei fail in exclusion of inert molecules. The indicated fluorescent proteins were added after nuclear assembly. They remained stably excluded from undepleted, or Nup62-depleted but not from WGA-depleted nuclei. The same result was obtained using fluorescent 70 kDa dextran that served as a passive exclusion marker in the other experiments of this study (Figure 2D).

(C) Nup62-depleted nuclei initiate DNA replication. Immunofluorescence was performed using rabbit anti-Nup107 and mouse anti-Nup62. Replication was monitored by incorporation of the fluorescent nucleotide analog Tetramethylrhodamin-5-dUTP (TMR-dUTP; added to 7.5 μM). As expected, replication was blocked by 25 μg/ml aphidicolin. WGA depletion also blocked replication – in agreement with Powers et al., 1995. Strikingly however, nuclei assembled in Nup62-depleted extracts showed a pattern of replication foci that was indistinguishable from that of control nuclei. Scale bar, 25 μm.

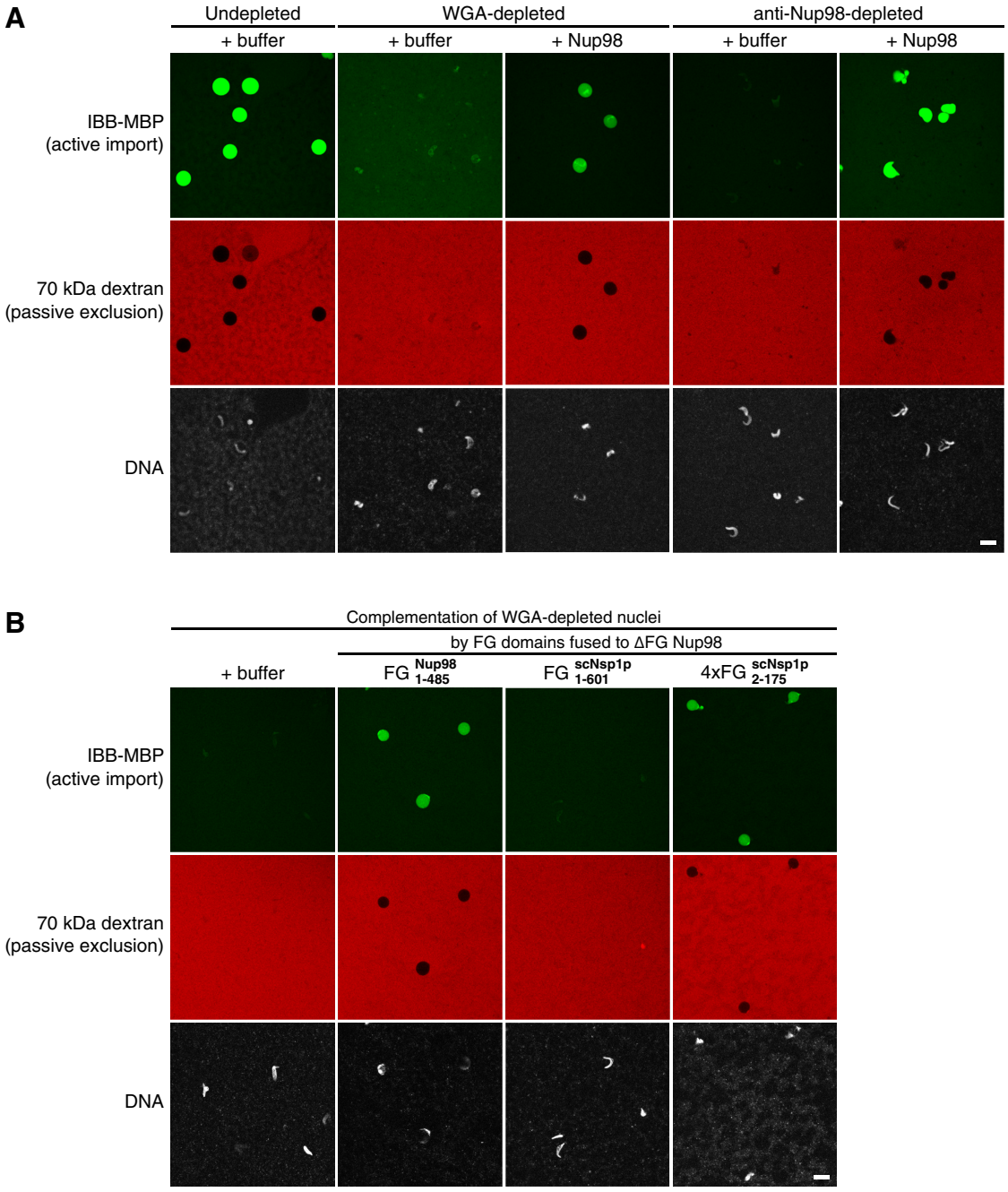

Figure S3. Functionality of Nuclei Imaged at Low Magnification, Related to Figures 4 and 7A

(A) Addition of Nup98 restores passive nuclear exclusion and active import in WGA- and Nup98-depleted nuclei. The experiment is identical to the one of Figure 4, but larger fields with more nuclei were imaged at lower magnification. Scale bar, 25 μm.

(B) Only FG domains that are cohesive along their entire sequence reconstitute a functional permeability barrier. The experiment is identical to the one of Figure 7A, but a larger field with more nuclei was imaged at lower magnification. Scale bar, 25 μm.

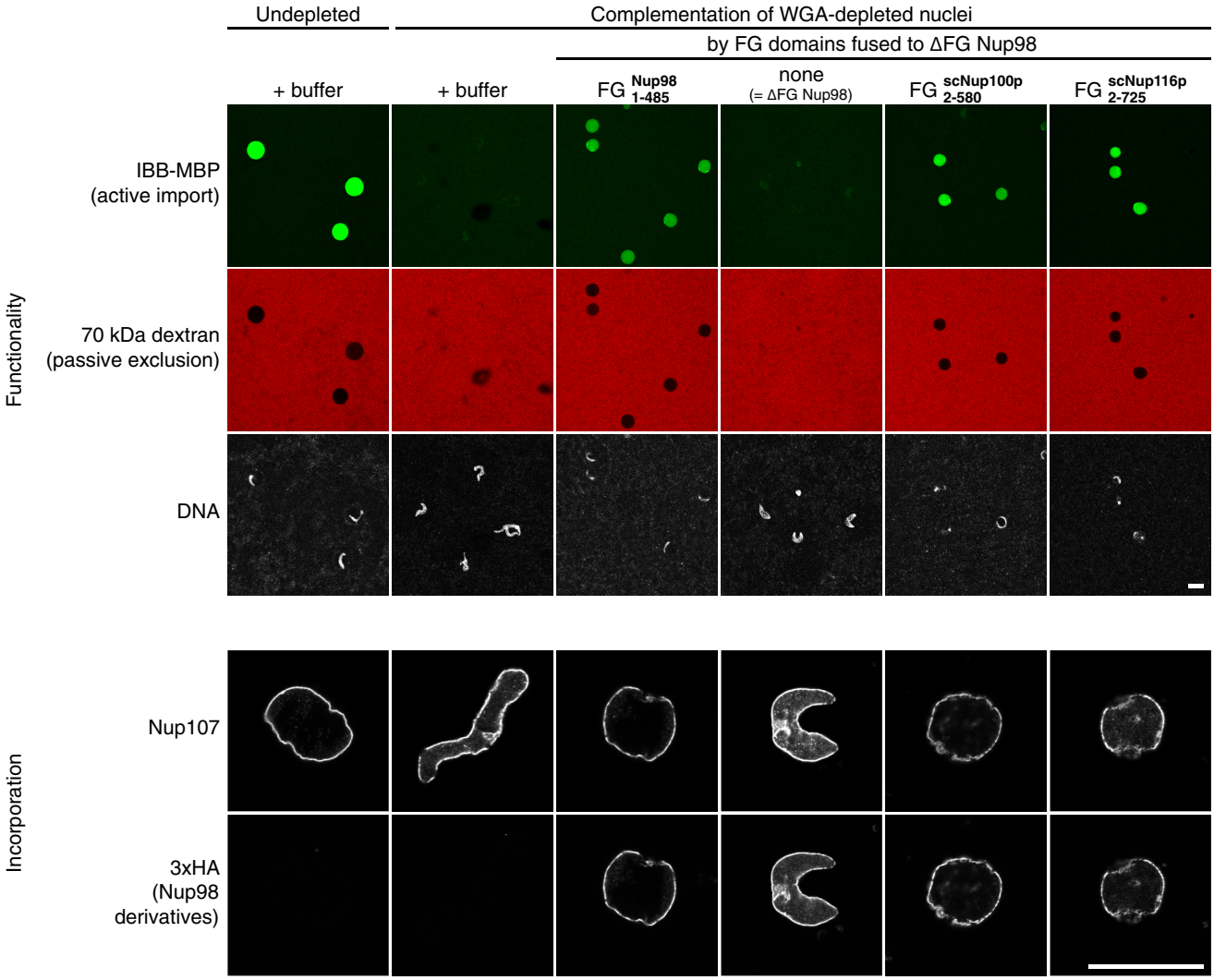

Figure S4. Cohesive FG Repeats of Yeast scNup100p and scNup116p Can Complement WGA-Depleted Nuclei, Related to Figure 6A

The functional experiment (upper panel) is identical to the one of Figure 6A, but a larger field with more nuclei was imaged at lower magnification. Scale bar, 25 μm. To test for incorporation of Nup98 variants (lower panel) nuclei were fixed and analyzed by immunofluorescence with anti-Nup107 and mouse anti-HA. Scale bar, 25 μm.

The efficiency of incorporation of 3xHA-tagged ΔFG Nup98 ("none") equaled that of similarly tagged Nup98 and Nup98 derivatives. Yet, in functional experiments it did not rescue the defects of WGA-depleted nuclei. Thus, operational NPCs required the anchorage of cohesive FG repeats from Nup98, scNup100p or scNup116p within the NPC channel.

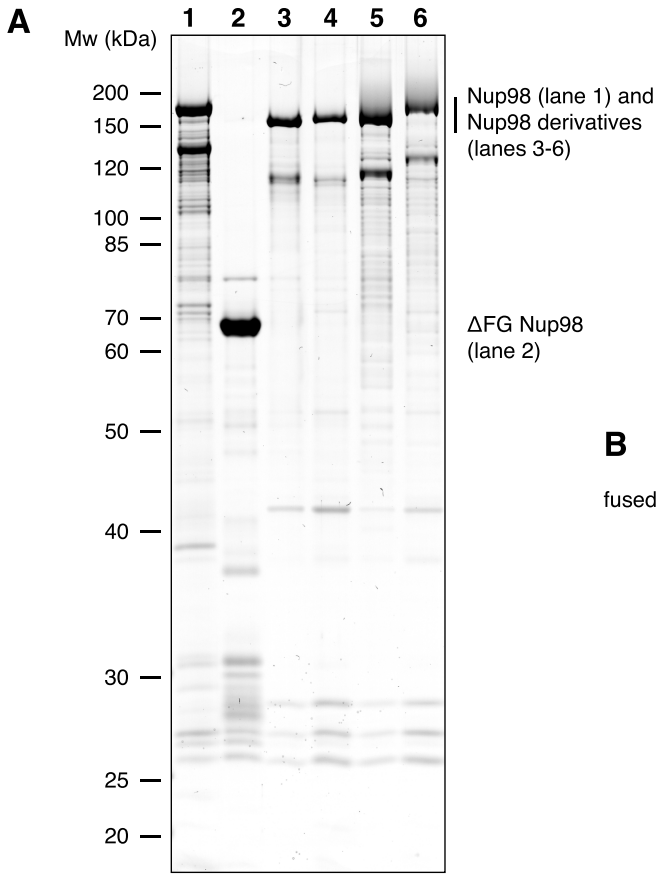

Lane	N-terminal tags and FG domains fused to ΔFG Nup98	Calc. Mw
1	His_{14}-MBP-SUMO-3xHA- FG $^{Nup98}_{1-485}$ -	150 kDa
2	His_{14}-3xHA -	52 kDa
3	His_{14}-3xHA- Φ⇒S FG $^{Nup98}_{1-485}$ -	95 kDa
4	His_{10}-LZ-3xHA- Φ⇒S FG $^{Nup98}_{1-485}$ -	97 kDa
5	His_{14}-3xHA- 2xFG $^{scNsp1p}_{274-601}$ -	121 kDa
6	His_{10}-LZ-3xHA- 2xFG $^{scNsp1p}_{274-601}$ -	123 kDa

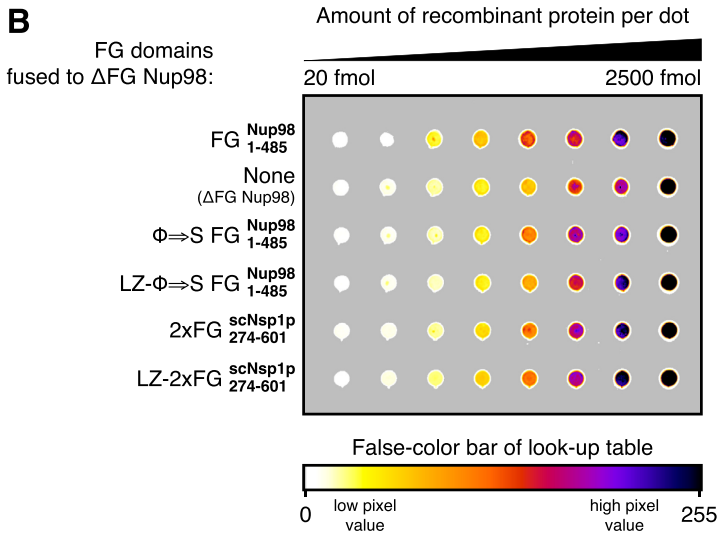

Figure S5. Analysis and Quantitation of Bacterially Expressed Nup98 Derivatives, Related to Figure 6C

Nup98 derivatives lacking FG repeats or containing non-cohesive ones were natively soluble when expressed with a simple oligo histidine tag. Derivatives with highly cohesive repeats, however, were soluble only with a very bulky N-terminal tag, such as a fusion between a His_{14}-tag, the maltose-binding protein (MBP) and SUMO.

(A) The SDS-PAGE analysis shows the purity of Nup98 derivatives used in this study. Please note that the Φ⇒S mutant of Nup98 FG repeats displays an unusual running behavior on SDS-PAGE because its mutations weaken SDS binding. The final preparations contain a certain amount of C-terminal truncations. However, because the NPC anchor of Nup98 is C-terminal (Hodel et al., 2002), only full-length proteins are incorporated into NPCs.

(B) The concentration of the corresponding full-length Nup98 derivatives was determined by immuno dot-blots, using an antibody against the Nup98 NPC anchor domain. ΔFG Nup98 served as a standard. Its concentration was measured photometrically at 280 nm, assuming a molar absorptivity of 42 500 $M^{-1} \cdot cm^{-1}$. The immuno dot-blot shown here is a re-validation following a successful quantification.

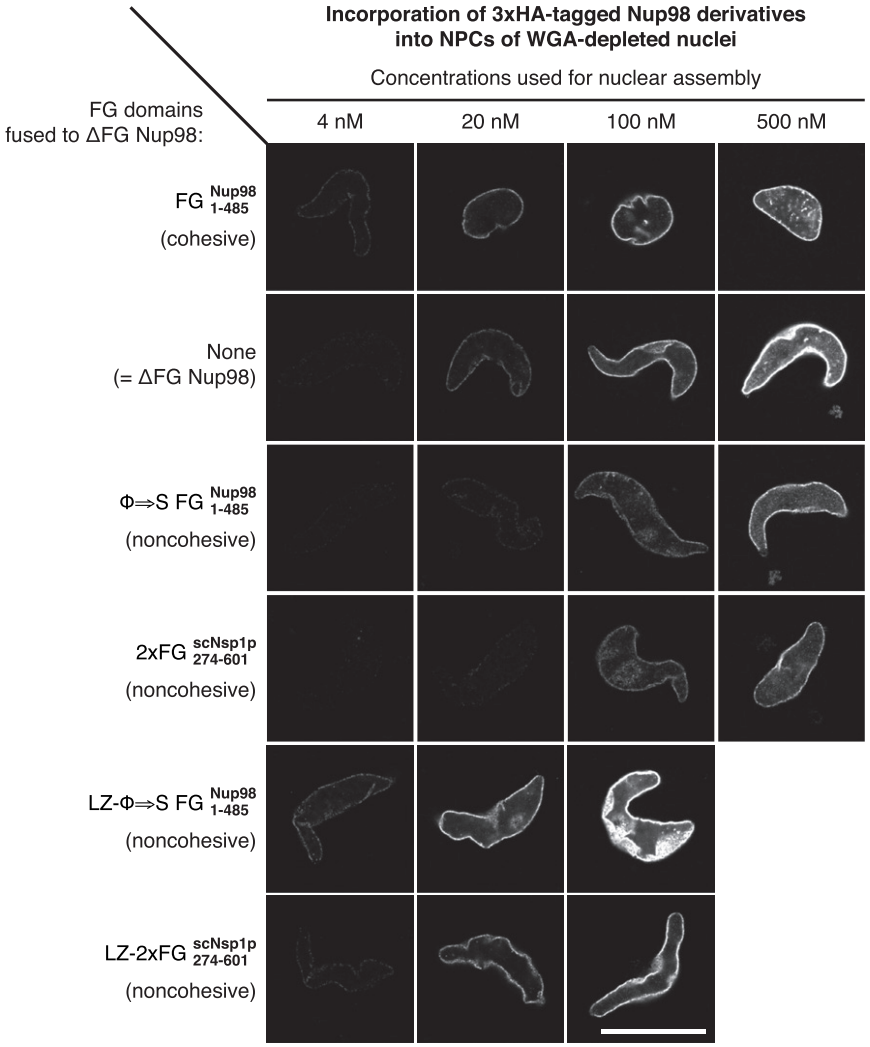

Figure S6. Comparing NPC Incorporation Efficiencies of Nup98 Derivatives, Related to Figure 6C

Nuclei were assembled from *Xenopus* sperm chromatin, membranes and WGA-depleted extract in the presence of increasing amounts of indicated Nup98 derivatives. Their incorporation into NPCs was assessed by anti-HA immunofluorescence. Nup98 derivatives with non-cohesive repeats required higher concentrations for efficient NPC-binding than wild-type Nup98. This inhibition of NPC-binding was overcome by fusion to a tetramerizing leucine zipper ("LZ"). Scale bar, 25 μm.

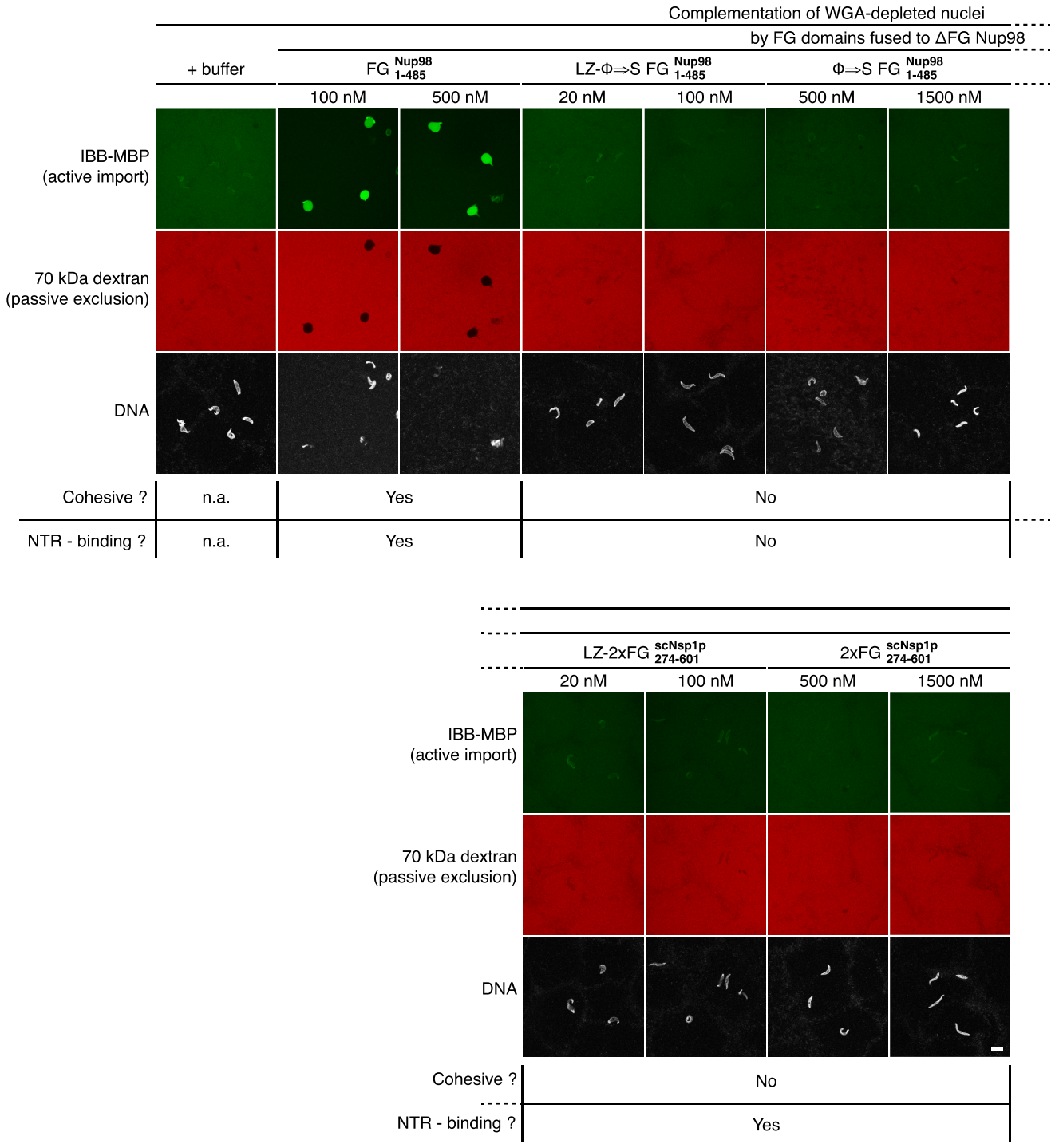

Figure S7. Complementation of WGA-Depleted Nuclei with Various Nup98 Derivatives, Related to Figure 6C

The experiment is identical to the one of Figure 6C, but larger fields with more nuclei were imaged at lower magnification, and additional titration points for Nup98 variants are shown. For the non-cohesive repeats, we tested an even wider range of concentrations than is shown here, but also these failed to restore a functional NPC barrier. Scale bar, 25 μm.